AD-A112 372 OHIO STATE UNIV COLUMBUS ELECTROSCIENCE LAB F/G 20/3
A UNIFORM GTD ANALYSIS OF THE SCATTERING OF ELECTROMAGNETIC WAV--ETC(U)
APR 79 P H PATHAK, W D BURNSIDE, R J MARHEFKA N62269-76-C-0554
UNCLASSIFIED ESL-784583-4 NL

1 of 1

END
DATE
FILMED
4-82
DTIC

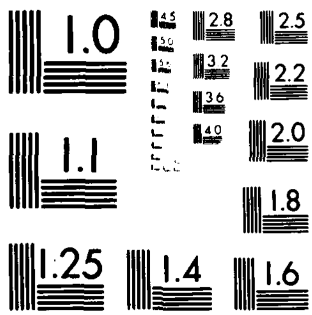

MICROCOPY RESOLUTION TEST CHART

PHOTOGRAPH THIS SHEET

AD-A112 372

DTIC ACCESSION NUMBER

II

LEVEL

INVENTORY

Ohio State Univ., Columbus
ElectroScience Lab.

A Uniform GTD Analysis of the Scattering of Electromagnetic Waves By A Smooth Convex Surface

DOCUMENT IDENTIFICATION

Apr. 79

Contract N62269-76-C-0554 Rept. No. ESL-784583-4

DISTRIBUTION STATEMENT A

Approved for public release;
Distribution Unlimited

DISTRIBUTION STATEMENT

ACCESSION FOR		
NTIS	GRA&I	☒
DTIC	TAB	☐
UNANNOUNCED		☐
JUSTIFICATION		
Per Ltr. on file		
FL-56, Acq# 81-2766,		
BY dtd. 4 Dec. '81.		
DISTRIBUTION /		
AVAILABILITY CODES		
DIST	AVAIL AND/OR SPECIAL	
A		

DISTRIBUTION STAMP

DTIC
SELECTED
MAR 24 1982
D

DATE ACCESSIONED

82 03 08 145

DATE RECEIVED IN DTIC

PHOTOGRAPH THIS SHEET AND RETURN TO DTIC-DDA-2

DTIC FORM OCT 79 70A

DOCUMENT PROCESSING SHEET

A UNIFORM GTD ANALYSIS OF THE SCATTERING OF ELECTROMAGNETIC WAVES BY A SMOOTH CONVEX SURFACE

OSU

P. H. Pathak, W. D. Burnside and R. J. Marhefka

The Ohio State University

ElectroScience Laboratory

Department of Electrical Engineering
Columbus, Ohio 43212

Technical Report 784583-4

Contract No. N62269-76-C-0554

April 1979

Department of the Navy
Naval Air Development Center
Warminster, Pennsylvania 18974

Enclosure (1)

NOTICES

When Government drawings, specifications, or other data are used for any purpose other than in connection with a definitely related Government procurement operation, the United States Government thereby incurs no responsibility nor any obligation whatsoever, and the fact that the Government may have formulated, furnished, or in any way supplied the said drawings, specifications, or other data, is not to be regarded by implication or otherwise as in any manner licensing the holder or any other person or corporation, or conveying any rights or permission to manufacture, use, or sell any patented invention that may in any way be related thereto.

SECURITY CLASSIFICATION OF THIS PAGE (When Data Entered)

REPORT DOCUMENTATION PAGE		READ INSTRUCTIONS BEFORE COMPLETING FORM
1. REPORT NUMBER	2. GOVT ACCESSION NO.	3. RECIPIENT'S CATALOG NUMBER
4. TITLE (and Subtitle) A UNIFORM GTD ANALYSIS OF THE SCATTERING OF ELECTROMAGNETIC WAVES BY A SMOOTH CONVEX SURFACE		5. TYPE OF REPORT & PERIOD COVERED Technical Report 6. PERFORMING ORG. REPORT NUMBER ESL 784583-4
7. AUTHOR(s) P. H. Pathak, W. D. Burnside and R. J. Marhefka		8. CONTRACT OR GRANT NUMBER(s) Contract N62269-76-C-0554
9. PERFORMING ORGANIZATION NAME AND ADDRESS Department of the Navy Naval Air Development Center Warminster, Pennsylvania 18974		10. PROGRAM ELEMENT, PROJECT, TASK AREA & WORK UNIT NUMBERS
11. CONTROLLING OFFICE NAME AND ADDRESS		12. REPORT DATE April 1979 13. NUMBER OF PAGES 54
14. MONITORING AGENCY NAME & ADDRESS(if different from Controlling Office)		15. SECURITY CLASS. (of this report) Unclassified 15a. DECLASSIFICATION/DOWNGRADING SCHEDULE

16. DISTRIBUTION STATEMENT (of this Report)

DISTRIBUTION STATEMENT A

Approved for public release;
Distribution Unlimited

17. DISTRIBUTION STATEMENT (of the abstract entered in Block 20, if different from Report)

18. SUPPLEMENTARY NOTES

19. KEY WORDS (Continue on reverse side if necessary and identify by block number)

Convex surface diffraction
Uniform GTD
Electromagnetic scattering

20. ABSTRACT (Continue on reverse side if necessary and identify by block number)

An approximate asymptotic high frequency solution is obtained for the field exterior to a smooth, perfectly conducting convex surface when it is excited by a ray optical electromagnetic field. This asymptotic solution is uniform in the sense that it is valid within the transition regions adjacent to the shadow boundaries where the pure ray optical solution based on the geometrical theory of diffraction (GTD) fails, and it reduces to the GTD solution in terms of the incident, reflected, and surface diffracted ray

20.

fields exterior to these transition regions where the GTD is indeed valid. This result employs the same ray paths as in the GTD solution, and it is expressed in the simple format of the GTD; hence, it is viewed as a uniform GTD solution. The construction of this uniform GTD solution is based on an asymptotic solution which was obtained previously for a simpler canonical problem. This uniform GTD solution can be conveniently and efficiently applied to many practical problems. It is shown that the numerical results based on this uniform GTD solution agree very well with experiments.

CONTENTS

I. INTRODUCTION

An approximate asymptotic high frequency solution is developed for the field exterior to a smooth, perfectly conducting convex surface when it is excited by a ray optical electromagnetic field. In the conventional GTD solution to this problem, the total field exterior to a surface is associated with the usual geometrical optics (GO) incident and reflected rays in the lit (or illuminated) region; whereas, in the shadow region it is associated entirely with the surface diffracted rays* introduced by Keller [1,2,3]. These rays are illustrated in Figure 1 together with the regions labeled I, II, III and V which divide the space exterior to the convex surface as follows. The shaded region II constitutes the transition region adjacent to the shadow boundary (SB of Figure 1) which divides the space exterior to the scatterer into the lit and shadow zones. The angular extent of region II is of the order of $(2/k\rho_g(Q_1))^{1/3}$ radians, where k is the wave-number of the homogeneous, isotropic medium exterior to the convex surface, and $\rho_g(Q_1)$ is the radius of curvature of the convex surface, in the plane containing the incident ray and the surface normal. The point of grazing incidence is specified by Q_1. The sub regions IV and VI in the shadow and lit zones, respectively, denote those portions of region II which are extremely close to the surface. In particular, regions IV and V are close to the portion of the surface which is a caustic of the surface diffracted rays; whereas, region VI is in the vicinity of Q_1 which is a caustic of the reflected ray for grazing incidence. Thus, regions IV, V and VI are commonly referred to as the caustic or surface boundary layer regions. The GTD is valid in regions I and III, but it fails in regions II and V.

*The surface diffracted rays are in general present even in the illuminated region if the surface is closed.

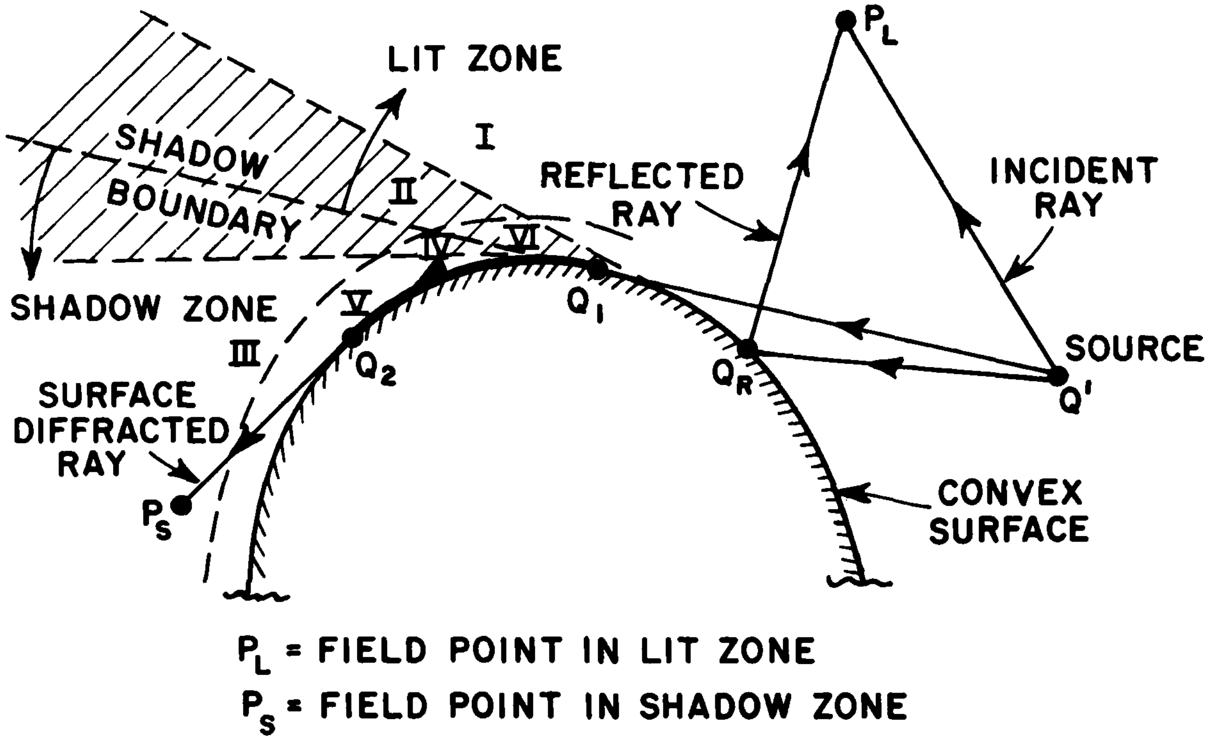

Figure 1. The rays and regions associated with scattering by a smooth convex cylinder.

An asymptotic analysis for the fields in regions II and V is complicated due to the fact that the asymptotic character of the field changes continuously but rapidly from one form to another across each of these regions. In this paper, an approximate uniform GTD (or UGTD) solution is developed which remains valid in regions I, III and the portion of region II which lies outside the sub regions IV and VI. An approximate asymptotic solution which is valid within the caustic boundary layer regions IV, V and VI is not considered in this work; it will be reported separately in the future.

The present ansatz or formulation of the uniform GTD solution is based on an asymptotic solution recently obtained by Pathak [4] for the canonical problem of plane wave scattering by a perfectly conducting circular cylinder. The work in [4] extends and improves some of our earlier work [5], and like most other analyses dealing with the diffraction by convex surfaces, this development draws upon the pioneering contributions of Fock [6]. The similarities and differences between the solution of the canonical problem in [4] and some of the other solutions which currently exist in the literature [7,8,9,10,11] are also discussed in [4]. The present ansatz based on the form of the solution of the canonical problem in [4] leads to a uniform GTD solution for an arbitrary convex surface which is convenient for engineering applications.

It is assumed here that the incident electromagnetic fields may be approximated locally by a quadratic ray pencil with a polarization which is transverse to the incident ray direction. One notes that plane, cylindrical, conical, and spherical type incident wavefronts are simply special cases of the arbitrary quadratic wavefront. It is further assumed in this paper that the field point location and the caustics of the incident ray pencil are not in the close vicinity of the surface, and that the amplitude of the incident ray optical field does not exhibit a rapid spatial variation in the vicinity of the points of reflection and diffraction on the convex surface. The details of this analysis are described in Sections II and III. First, a brief review of the GTD solution for this general problem of the scattering of an arbitrary ray optical electromagnetic field by a smooth, perfectly-conducting convex surface is presented in Section II for the sake of completeness. A uniform GTD solution to this problem is developed next in Section III. Several examples illustrating the usefulness and accuracy of this uniform GTD solution are presented in Section IV.

II. THE GTD SOLUTION - A REVIEW

This review serves to introduce the GTD format and notation that will be employed in the development of the uniform GTD solution.

The incident ray system which strikes the convex surface produces a system of rays reflected from that surface, and the field of these incident and reflected rays constitutes the usual geometrical optics (GO) field. The reflected ray merges with the incident ray at grazing forming a shadow boundary which divides the space exterior to the convex surface into the lit and shadow regions, as shown in Figure 1. At grazing, the incident field launches Keller's surface rays which propagate along geodesic paths on the convex surface while continually shedding energy via diffraction along the forward tangents to the surface ray paths. The field of these rays which are shed (or diffracted) from the surface is known as the surface diffracted field. The GO field is zero within the shadow region behind the obstacle; thus, the field within the shadow zone is produced entirely by the surface diffracted rays. These surface diffracted rays may also be present in the lit region if the surface of the obstacle is closed; however, this field is generally negligible compared to the GO field if the closed surface is sufficiently large in terms of the wavelength.

The GO solution for the lit region is briefly reviewed in part A of this section. A brief review of the surface diffracted ray solution for the shadow zone is presented next in part B. An $\exp(j\omega t)$ time dependence is is assumed in this analysis.

A. The Geometrical Optics Field Solution for the Lit Region

Luneberg [12] and Kline [13] developed an asymptotic high frequency solution of Maxwell's equations in which the fields are expanded in inverse powers of the angular frequency, ω. The leading term in this expansion is regarded as the GO field. The details of such an expansion are discussed elsewhere [12,13,14,15] and are only summarized here. According to Luneberg and Kline, the electric field intensity, $\overline{E}$ in a source free, homogeneous, isotropic medium can be expressed for large ω by

$$\overline{E}(\overline{r},\omega) \sim e^{-jk\psi(\overline{r})} \sum_{n=0}^{\infty} \frac{\overline{E}_n(\overline{r})}{(-jk)^n} \quad , \tag{1}$$

in which $\overline{r}$ is the position vector of the field point; $k = \omega/c$; and c is the speed of light in the given medium. The coefficients $\overline{E}_n(\overline{r})$ in the above expansion are determined by substituting Equation (1) into the vector Helmholtz equation satisfied by $\overline{E}$; namely, $(\nabla^2 + k^2)\,\overline{E} = 0$, and by equating like powers of ω. This leads to the usual eikonal and transport equations; namely, $|\nabla\psi|^2 = 1$ and $|\nabla^2\psi + 2\nabla\psi\cdot\nabla|\ \overline{E}_n = -\nabla^2\overline{E}_{n-1}$ (with $E_{-1} = 0$), respectively. The surfaces of constant ψ are referred to as wavefronts, and the family of all wavefronts describe a system of associated rays which are straight lines in a homogeneous medium. The rays are everywhere orthogonal to the wavefronts in an isotropic medium. Integrating the transport equation for the n=0 case from some reference point $\overline{r}_0$ to the field point $\overline{r}$, and expressing this result in terms of the Gaussian curvatures of the wavefronts at $\overline{r}_0$ and $\overline{r}$ yields the GO field:

$$\overline{E}^{i,r}(\overline{r}) \sim \overline{E}_0^{i,r}(\overline{r}_0)\ e^{-jk\psi^{i,r}(\overline{r}_0)} \sqrt{\frac{\rho_1^{i,r}\ \rho_2^{i,r}}{(\rho_1^{i,r} + s^{i,r})(\rho_2^{i,r} + s^{i,r})}}\ e^{-jks^{i,r}} . \tag{2}$$

The superscripts "i" and "r" refer to the incident and reflected GO fields, respectively; thus, $\overline{E}^i$ is the incident GO field and $\overline{E}^r$ is the reflected GO field. Note that $\rho_1^{i,r}$ and $\rho_2^{i,r}$ are the principal radii of curvatures of the incident or reflected wavefront surface dA_0 at $\overline{r}_0$, and $s^{i,r}$ is the distance along the incident or reflected ray from $\overline{r}_0$ to $\overline{r}$ as shown in Figure 2. Next, requiring $\nabla\cdot\overline{E} = 0$ leads to $(\hat{s}^{i,r}\cdot\overline{E}_0^{i,r}) = 0$, which implies that the field in Equation (2) is polarized transverse to the ray directions $(\hat{s}^{i,r})$ as shown in Figure 3. The quantity involving the square root in Equation (2) is the ray divergence factor which indicates the manner in which the energy spreads along the ray path; it is a consequence of the conservation of energy in a ray tube (or pencil). From Maxwell's equation $\nabla\times\overline{E} = -j\omega\mu\overline{H}$, it follows that the leading term in the Luneberg-Kline expansion for the corresponding

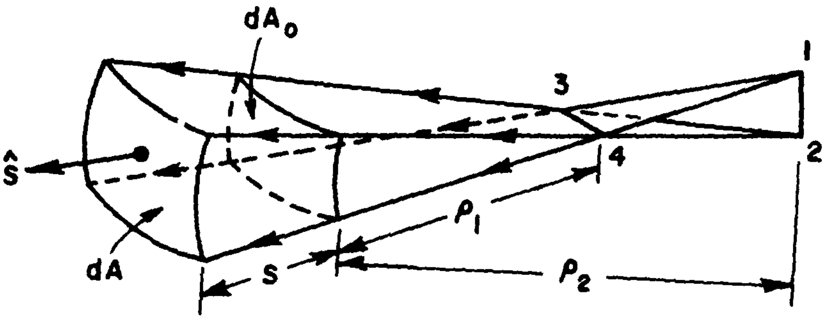

$\hat{S}$ = UNIT VECTOR ALONG THE CENTRAL OR AXIAL RAY

dA$_o$ IS THE INCREMENTAL WAVEFRONT AREA OF THE RAY PENCIL AT THE REFERENCE POINT $\bar{r}_o$

dA IS THE INCREMENTAL WAVEFRONT AREA OF THE RAY PENCIL AT THE FIELD POINT $\bar{r}$

Figure 2. Astigmatic tube of rays.

magnetic field intensity is $\overline{H}^{i,r} \sim \hat{s}^{i,r} \times Y_o \overline{E}^{i,r}$ in which $\overline{E}^{i,r}$ is as given in Equation (2), and Y_o is the characteristic admittance of the medium. From the boundary condition $\hat{n} \times [\overline{E}^i + \overline{E}^r] = 0$ on the perfectly-conducting surface, where $\hat{n}$ is the surface normal at the point of reflection Q_R as shown in Figure 3, one obtains

$$\overline{E}^r(Q_R) = \overline{E}^i(Q_R) \cdot \bar{\bar{R}} \quad . \tag{3}$$

Thus, the reflected GO field is given in terms of the incident field at Q_R as

$$\overline{E}^r(\overline{r}) \sim \overline{E}^i(Q_R) \cdot \bar{\bar{R}} \sqrt{\frac{\rho_1^r \rho_2^r}{(\rho_1^r+s^r)(\rho_2^r+s^r)}} \; e^{-jks^r} \quad , \tag{4}$$

$$\bar{\bar{R}} = [R_s \, \hat{e}_\perp \, \hat{e}_\perp + R_h \, \hat{e}_\parallel^i \, \hat{e}_\parallel^r] \; ; \qquad R_{\substack{s \\ h}} = \mp 1 \tag{5a;5b}$$

where $\bar{\bar{R}}$ is the dyadic reflection coefficient, and ρ_1^r, ρ_2^r, and s^r are measured with respect to the reference point $\overline{r}_o$ which is now moved to Q_R. R_s and R_h are the acoustic soft and hard reflection coefficients, respectively. The unit vector $\hat{e}_\perp$ in Equation (5a) is perpendicular to the plane of incidence; whereas, the unit vectors $\hat{e}_\parallel^i$ and $\hat{e}_\parallel^r$ are in the plane of incidence as shown in Figure 3. The principal radii of curvatures (ρ_1^r, ρ_2^r) of the reflected wavefront and their associated principal directions $(\hat{X}_1^r, \hat{X}_2^r)$ are described in Reference [16]. The ρ_1^r and ρ_2^r as given in [16] are expressed more compactly below:

$$\frac{1}{\rho^r_{\frac{1}{2}}} = \frac{1}{\rho^i_m} + \frac{f}{\rho_g(Q_R)\cos\theta^i}\left(1 \pm \left[\frac{\rho_g^2(Q_R)\cos^2\theta^i}{4f^2}\left(\frac{1}{\rho^i_1} - \frac{1}{\rho^i_2}\right)^2 + \frac{\rho_g^2(Q_R)\cos\theta^i}{f^2}\left(\frac{1}{\rho^i_1} - \frac{1}{\rho^i_2}\right)\cdot\right.\right.$$

$$\left.\left.\cdot\left\{\frac{g\cos 2\alpha_o}{\rho_g(Q_R)} - \sin 2\alpha_o \sin 2\omega_o \cos\theta^i\left(\frac{1}{R_1} - \frac{1}{R_2}\right)\right\} + 1 - \frac{4\rho_g^2(Q_R)\cos^2\theta^i}{f^2 R_1 R_2}\right]^{1/2}\right), \tag{6a}$$

where

$$\frac{1}{\rho^i_m} = \frac{1}{2}\left(\frac{1}{\rho^i_1} + \frac{1}{\rho^i_2}\right) \quad ; \quad \begin{Bmatrix} f \\ g \end{Bmatrix} = \left\{1 \pm \frac{\rho_g(Q_R)}{\rho_t(Q_R)}\cos^2\theta^i\right\}. \tag{6b;6c}$$

The quantities ρ^i_1 and ρ^i_2 constitute the principal radii of curvatures of the incident wavefront. In Equation (6a), ρ^r_1 and ρ^r_2 are evaluated at the point of reflection Q_R on the surface. R_1 and R_2 constitute the principal radii of curvatures of the surface at Q_R, and $\hat{U}_1$ and $\hat{U}_2$ denote the corresponding principal surface directions at Q_R. The radius of curvature of the surface at Q_R is ρ_g; it is measured in the plane of incidence which contains $\hat{s}^i$, $\hat{n}$ and $\hat{t}$, where $\hat{t}$ is tangent to the surface. Also, ρ_t is the radius of curvature of the surface at Q_R in the plane containing $\hat{n}$ and the binormal vector $\hat{b}$. The unit vectors $\hat{t}$, $\hat{n}$, $\hat{b}$, $\hat{U}_1$ and $\hat{U}_2$ are shown in Figure 4a together with the angle ω_o between $\hat{t}$ and $\hat{U}_2$. The unit vectors $\hat{X}^i_1$, $\hat{X}^i_2$, and the angle α_o are shown in Figure 4b. The angle of incidence, θ^i is defined by $\hat{n}\cdot\hat{s}^i = -\cos\theta^i = -\hat{n}\cdot\hat{s}^r$.

It is noted that the GO representation of Equation (2) fails at caustics which are the intersection of the paraxial rays (comprising the ray tube or pencil) at the lines 1-2, and 3-4 as shown in Figure 2. Upon crossing a caustic in the direction of propagation, $(\rho^{i,r} + s^{i,r})$ changes sign under the radical in Equation (2), and a phase jump of $+\pi/2$ results (for $e^{+j\omega t}$ time dependence). Furthermore, the reflected GO field, $\bar{E}^r$ of Equation (4)

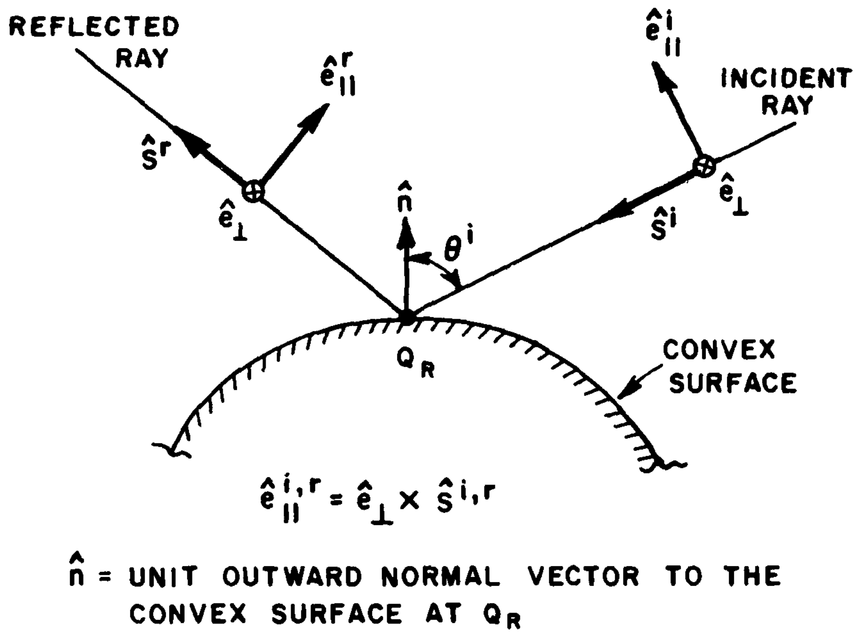

Figure 3. Reflection by a curved surface.

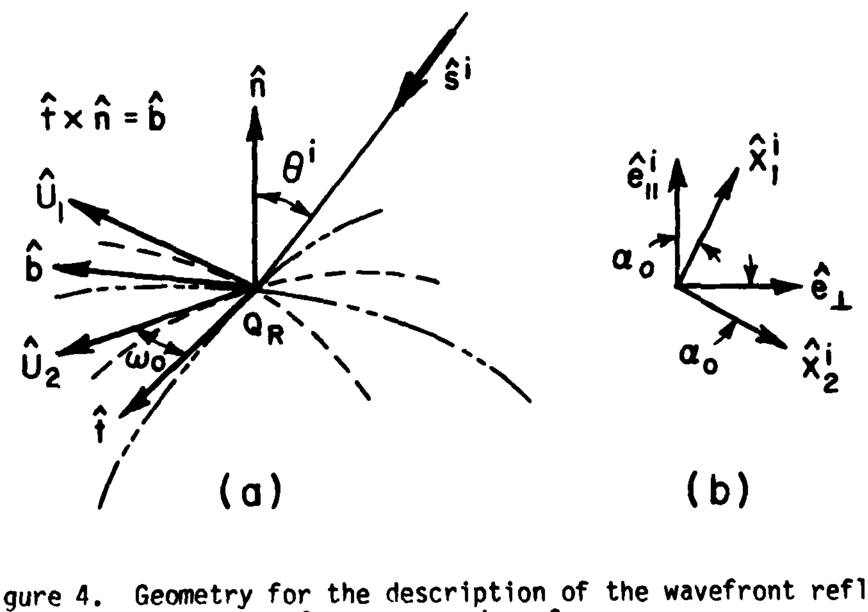

Figure 4. Geometry for the description of the wavefront reflected from a curved surface.

fails at and near grazing incidence. However, it is important to note that near grazing incidence ($\theta^i \to \pi/2$), ρ_1^r and ρ_2^r of Equation (6) approach the following limiting values.

$$\rho_1^r \to \frac{\rho_g(Q_R)\cos\theta^i}{2} \to 0; \qquad \rho_2^r \to \rho_b^i , \tag{7a;7b}$$

where

$$1/\rho_b^i = (\sin^2\alpha_o/\rho_1^i) + (\cos^2\alpha_o/\rho_2^i), \tag{8}$$

and ρ_b^i is the radius of curvature of the incident wavefront in the $(\hat{t},\hat{b})$ plane (i.e., in the plane tangent to the surface) at Q_R for $\theta^i \to \pi/2$. Furthermore, the principal directions $\hat{X}_1^r$ and $\hat{X}_2^r$ of the reflected wavefront approach the following values for grazing incidence:

$$\hat{X}_1^r \to \hat{n} \text{ (at } Q_R) \; ; \qquad \hat{X}_2^r = (-\hat{s}^r \times \hat{X}_1^r) \to \hat{b} \text{ (at } Q_R) \; . \tag{9a;9b}$$

The limiting values in Equation (9a;b) are independent of α_o. The total GO field, $\overline{E}$ at P_L (see Figure 1) in the lit region is the sum of the incident and reflected GO ray fields; hence,

$$\overline{E}(P_L) \sim \overline{E}^i(P_L) + \overline{E}^i(Q_R) \cdot \bar{\bar{R}} \sqrt{\frac{\rho_1^r \rho_2^r}{(\rho_1^r+s^r)(\rho_2^r+s^r)}} \; e^{-jks^r} \; . \tag{10}$$

B. <u>The Surface Diffracted Ray Field Solution for the Shadow Region</u>

The incident ray at grazing launches a set of surface rays which propagate along a geodesic path on the convex surface thereby carrying energy into the shadow region. The field associated with these surface rays attenuates (i.e., decays exponentially) as they propagate due to a continuous shedding (diffraction) of rays along the forward tangents to the geodesic ray path, as shown in Figure 5. An analysis of this surface diffracted field is discussed in detail elsewhere [1,2,15]; hence, only the essential features are summarized here. Let $\hat{n}_1$ and $\hat{t}_1$ denote the unit normal and tangent vectors at the point of grazing incidence, Q_1; likewise, let $\hat{n}_2$ and $\hat{t}_2$ denote the unit normal and tangent vectors, respectively, at the point of tangential shedding of the surface diffracted ray at Q_2. The diffracted ray pencil possesses caustics at Q_2 and P_c as seen in Figure 5; these caustics are the same as those at 3-4 and 1-2 of the typical ray pencil in Figure 2. The diffracted electric field $\bar{E}^d$ arriving at P_s may be represented as a ray optical field; hence $\bar{E}^d$ is given by Equation (2) with the superscripts "i,r" replaced by "d" to denote the "diffracted" ray. Then ρ_1^d and ρ_2^d become the caustic distances associated with the diffracted wavefront at some reference point ($\bar{r}_o$) which lies between Q_2 and P_s, as in Figure 2. However, if the reference position $\bar{r}_o$ is moved back to the caustic at Q_2, then $\rho_1^d \to 0$, and ρ_2^d now becomes the distance from Q_2 to P_c. Let

$$\lim_{\rho_1^d \to 0} \bar{E}^d(\bar{r}_o) e^{-jk\psi^d(\bar{r}_o)} \sqrt{\rho_1^d} = \bar{E}^i(Q_1) . \bar{\bar{T}}(Q_1,Q_2) \quad . \tag{11}$$

Therefore, the electric field ($\bar{E}^d$) at a point P_s in the shadow region (see Figure 1) becomes

$$\bar{E}^d(P_s) \sim \bar{E}^i(Q_1) \cdot \bar{\bar{T}}(Q_1,Q_2) \sqrt{\frac{\rho_2^d}{s^d(\rho_2^d+s^d)}} \; e^{-jks^d} \quad . \tag{12a}$$

$\bar{\bar{T}}(Q_1,Q_2)$ is a "dyadic transfer function" which relates the field diffracted from Q_2 to the field incident at Q_1. This dyadic quantity is expressed as [3,15]

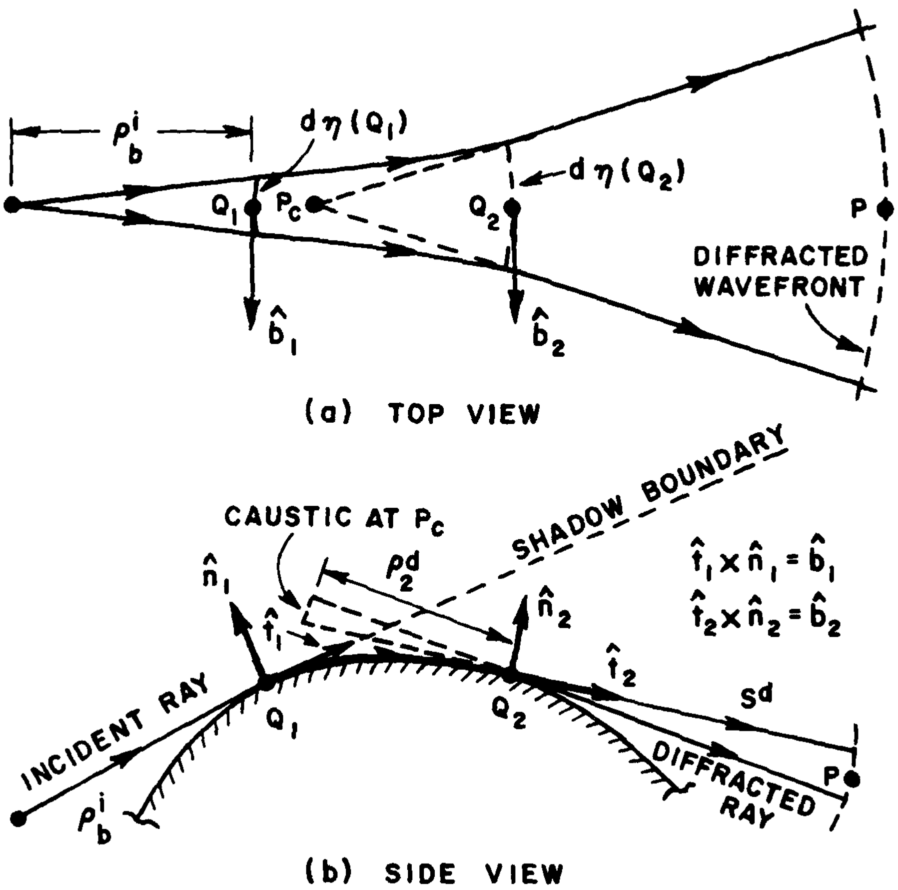

Figure 5. Diffraction by a smooth curved surface.

$$\bar{T}(Q_1,Q_2) = \hat{b}_1\hat{b}_2\, T_s + \hat{n}_1\hat{n}_2\, T_h \quad , \tag{12b}$$

in which

$$T_{\substack{s\\h}} = \sum_{P=1}^{N} D_p^{\substack{s\\h}}(Q_1) \left[e^{-jkt-\int_{Q_1}^{Q_2} \alpha_p^{\substack{s\\h}}(t')dt'} \sqrt{\frac{d\eta(Q_1)}{d\eta(Q_2)}} \right] D_p^{\substack{s\\h}}(Q_2) \quad , \tag{12c}$$

and t is the geodesic arc length from Q_1 to Q_2 on the surface. It is clear from Equation (12b) that the ray field in Equation (12a) is polarized transverse to the ray path. It is assumed in Equations (12a;b) that the $\hat{n}_2$ and $\hat{b}_2$ components of $\bar{E}^d$ propagate independently of each other. The sum in Equation (12c) indicates that the surface ray field is actually composed of a set of surface ray modes as indicated earlier, and p refers to the modal index. The superscripts s and h in Equations (12b;c) denote the acoustic soft and hard type field contributions, respectively. $D_p^{\substack{s\\h}}(Q_1)$ are referred to as the surface dif-fraction coefficients which describe the diffraction at Q_1. The forms of $D_p^{\substack{s\\h}}(Q_1)$ and $D_p^{\substack{s\\h}}(Q_2)$ must be identical via reciprocity. The factor

$$\sqrt{\frac{d\eta(Q_1)}{d\eta(Q_2)}}\; e^{-jkt - \int_{Q_1}^{Q_2} \alpha_p^{\substack{s\\h}}(t')dt'}$$

is the ratio of the surface ray field incident at Q_2 (prior to diffraction from Q_2) to the surface ray field launched by the incident field at Q_1. This factor is obtained by integrating

$$\frac{d}{dt}\left(a_{\substack{s\\h}}^2\, d\eta\right) = -\,2\left(\alpha_p^{\substack{s\\h}}\, a_{\substack{s\\h}}^2\, d\eta\right) \quad ,$$

from Q_1 to Q_2, with $a^2_{s,h}$ being the intensity of the p^{th} soft and hard surface ray field and dt is the incremental arc length between Q_1 and Q_2. This expression is based on the assumption that energy is conserved in the surface ray pencil between Q_1 and Q_2, and that the surface ray decays exponentially with an attenuation coefficient $\alpha_p^{s,h}$. The factor e^{-jkt} denotes the dominant phase delay of the surface ray field from Q_1 to Q_2.

The form of the solution in Equations (12a;b;c) has been verified via asymptotic solutions to appropriate canonical problems [3,17]; also, these canonical solutions lead to the specific expressions for $D_p^{s,h}$ and $\alpha_p^{s,h}$ which to first order are given by [3,17]

$$\left[D_p^s\right]^2 = \sqrt{\frac{1}{2\pi k}}\left(\frac{k\rho_g}{2}\right)^{1/3} \frac{e^{-j\frac{\pi}{12}}}{\left[Ai'(-q_p)\right]^2} \; ; \quad \left[D_p^h\right]^2 = \sqrt{\frac{1}{2\pi k}}\left(\frac{k\rho_g}{2}\right)^{1/3} \frac{e^{-j\frac{\pi}{12}}}{\bar{q}_p\left[Ai(-\bar{q}_p)\right]^2} \tag{13a;13b}$$

$$\alpha_p^s = \frac{q_p}{\rho_g}\left(\frac{k\rho_g}{2}\right)^{1/3} e^{j\frac{\pi}{6}} \; ; \quad \alpha_p^h = \frac{\bar{q}_p}{\rho_g}\left(\frac{k\rho_g}{2}\right)^{1/3} e^{j\frac{\pi}{6}} . \tag{14a;14b}$$

The Ai and Ai' denote the Keller type Airy function and it's derivative [3,15] respectively. The values q_p and $\bar{q}_p$ are those for which $Ai(-q_p) = 0$ and $Ai'(-\bar{q}_p) = 0$. The values of $Ai(-\bar{q}_p)$ and $Ai'(-q_p)$ are given in [9,18]. It is noted that ρ_g refers to the surface radius of curvature in the ray direction (i.e., in the $\hat{n},\hat{t}$ plane). In Equation (12c), the inclusion of only the first couple of modes (i.e., p=1,2) is sufficient for obtaining accurate results in the deep shadow region. However, the result in Equations (12a;b;c) fails at and near the shadow boundary; it also fails near the caustic at Q_2.

III. THE CONSTRUCTION OF A UNIFORM GTD SOLUTION

The GTD solution of Section II fails at and near the shadow boundary because the GTD ray optical field description is not valid there. Consequently, one must employ a uniform asymptotic field approximation which remains valid within the shadow boundary transition region. A uniform theory must therefore basically depart from the pure ray optical field approximation inherent in the GTD in order to correct for the failure of the GTD within the shadow boundary (SB) transition region; whereas, away from this SB transition region, it must reduce to the usual GTD solution where the latter is indeed valid. The precise manner in which a uniform theory accomplishes such a task differs with each ansatz. While different formulations of uniform solutions might even lead to the same answers exactly at the SB, and also exterior to the SB transition region where they all must reduce to the GTD solution, their behavior within the transition region may not necessarily be the same.

As mentioned in Section I, the ansatz employed in this paper is based on an asymptotic solution given by Pathak [4] for the canonical problem of plane wave scattering by a smooth, perfectly-conducting convex cylinder. This ansatz leads to a *uniform GTD solution for the general* problem of the scattering of a ray optical electromagnetic field by a smooth, perfectly-conducting convex surface of any shape, such that the solution thus obtained is convenient and accurate for engineering applications. The starting point in the development of this general solution is the uniform result given in Equations (A-16a;b) of the Appendix, for the far zone fields of a scalar point source radiating in the presence of an acoustic soft or hard, smooth convex cylinder. The result in Equations (A-16a;b) is developed in the Appendix from the uniform asymptotic solution of the canonical problem of [4], the latter solution is also summarized in Equations (A-1a;b) of the Appendix. The reader is referred to the Appendix for details.

First, it is observed that the uniform result in Equations (A-16a;b) is already in the convenient ray type format; however, the field itself is not a ray optical field within the SB transition region. The scattered field in Equations (A-16a;b) propagates along the GO reflected ray path in the lit region (which also includes the lit portion of the SB transition region), and it propagates along the surface diffracted ray path in the shadow region (including the shadowed portion of the SB transition region). This uniform result properly reduces to the GO soft or hard type ray field solution in the lit region which lies outside the SB transition region, and also to the soft or hard type surface diffracted ray field solution in the shadow region which lies exterior to the SB transition region. The preceding reduction to the GTD solution is easily verified by noting that the F and $\hat{P}_{\substack{s\\h}}$ functions which occur in Equations (A-16a;b) of the Appendix take the following limiting values, when the field point moves exterior to the SB transition region:

$$[1-F(\sigma)] \to 0 \quad , \qquad \text{for } \sigma >> 0 \left(\begin{array}{l}\text{which is true both, in the lit and}\\ \text{shadow zones exterior to the SB}\\ \text{transition region.}\end{array}\right) \tag{15}$$

$$\hat{P}_{\substack{s\\h}}(\delta) \sim \pm \left\{\begin{array}{c} R_{\substack{s\\h}} \end{array}\right\} \sqrt{\frac{-\delta}{4}}\, e^{j\frac{\delta^3}{12}} \quad , \qquad \text{for } \delta << 0 \left(\begin{array}{l}\text{which is true in the lit zone}\\ \text{exterior to the SB transition}\\ \text{region.}\end{array}\right) \tag{16a}$$

$$\left.\begin{aligned}\hat{P}_s(\delta) &\sim -\frac{e^{-j\frac{\pi}{4}}}{\sqrt{\pi}}\sum_{P=1}^{N}\frac{e^{j\frac{\pi}{6}}\,e^{\delta q_p e^{-j\frac{5\pi}{6}}}}{2[Ai'(-q_p)]^2}\\ \hat{P}_h(\delta) &\sim -\frac{e^{-j\frac{\pi}{4}}}{\sqrt{\pi}}\sum_{P=1}^{N}\frac{e^{j\frac{\pi}{6}}\,e^{\delta \overline{q}_p e^{-j\frac{5\pi}{6}}}}{2\,\overline{q}_p[Ai(-\overline{q}_p)]^2}\end{aligned}\right\}\ \text{for } \delta>>0 \begin{pmatrix}\text{which is true in}\\ \text{the shadow zone}\\ \text{exterior to the SB}\\ \text{transition region.}\end{pmatrix} \qquad (16b)$$

The N in the summation of Equation (16b) is identical to the N in Equation (12c); it is noted that N=2 generally provides sufficient accuracy when $\delta>>0$. Furthermore, the limit of the result in Equation (A-16a) as the field point approaches SB from the lit side is identical to the limit of the result in Equation (A-16b) as the field point approaches SB from the shadow side; thus, the total field is continuous across SB. It is noted that as the field point approaches SB:

$$F(\sigma) \approx \left[\,|\sqrt{\pi\sigma}| - 2\sigma\, e^{j\frac{\pi}{4}}\right] e^{j(\frac{\pi}{4}+\sigma)}, \qquad \text{for } \sigma\to 0 \ (\sigma=0 \text{ on SB}). \qquad (17)$$

Also, the limiting value of the field at the SB is more easily evaluated if one defines $\hat{P}_{\substack{s\\h}}(\delta)$ in terms of the related functions $p^*(\delta)$ and $q^*(\delta)$ as in [4]:

$$\hat{P}_{\substack{s\\h}}(\delta) = \begin{Bmatrix} p^*(\delta)\\ q^*(\delta)\end{Bmatrix} e^{-j\frac{\pi}{4}} - \frac{e^{-j\frac{\pi}{4}}}{2\sqrt{\pi}\delta}, \qquad \text{(Note that } \delta=0 \text{ at SB).} \qquad (18)$$

From the above limiting forms of $F(\sigma)$ and $\hat{P}_{\substack{s\\h}}(\delta)$, one notes that the $F(\sigma)$ term in Equations (A-16a;b) plays a dominant role in the immediate neighborhood of SB, and it is entirely responsible for ensuring the continuity of the total field at SB. On the other hand the $\hat{P}_s^h(\delta)$ term in Equations (A-16a;b) plays a dominant role as the field point moves far from SB (since $|1-F(\sigma)| \to 0$), and it is therefore entirely responsible for reducing Equations (A-16a;b) uniformly to the GTD solution, exterior to the SB transition region, for the case of the far zone field of a scalar point source radiating in the presence of an acoustic soft or hard convex cylinder. A more complete discussion on the role of the functions F and $\hat{P}_s^h$ is given in Reference [4], in connection with the development of a uniform asymptotic solution to the canonical problem of plane wave scattering by a convex cylinder. It is important to note that the F function involves a Fresnel integral which is well tabulated; and $\hat{P}_s^h$ is a Fock type integral (involving Airy functions) which is also tabulated.

It is observed that the GTD solution of Section II, which is a first order asymptotic solution to terms in inverse powers of $k\rho_g$, is valid for cylindrical, spherical, or any other smooth convex shape. It is also valid for torsional surface rays in that effects of torsion do not occur explicitly to first order for the scattering problem considered here. In addition, it is observed that a simple relationship exists in the GTD solution between the vector electromagnetic and the scalar acoustic problems to the given order of approximation; namely, $\bar{\bar{R}}$ and $\bar{\bar{T}}$ of the GTD solution in Equations (5a;b) and (12a;b) are a simple combination of the corresponding scalar or acoustic (soft and hard) functions R_s^h, and T_s^h for the lit and shadow regions, respectively. The last two observations in regard to the GTD solution including it's validity for torsional surface rays have been verified via the rigorous asymptotic solutions to several canonical problems [3,18]. Based on these observations and the previous observation that the uniform asymptotic result in Equations (A-16a;b) of the Appendix dealing with the far zone field of a point source radiating in the presence of an acoustic soft or hard convex cylinder is already in a ray format, it is reasonable to conjecture the following in regard to the uniform GTD solution:

(a) The uniform GTD solution for the general electromagnetic problem of the scattering of a ray optical electromagnetic field incident on a smooth, perfectly-conducting arbitrary convex surface can also be expressed in a ray type format like the ordinary GTD solution of Section II (see Equations (10) and (12a)).

(b) The dyadics $\bar{R}$ and $\bar{T}$ in Equations (5a;b) and (12a;b) of the ordinary GTD solution may be replaced by the more general $\bar{\bar{R}}$ and $\bar{\bar{T}}$ dyadics for the uniform GTD solution. Of course, $\bar{\bar{R}} \to \bar{R}$ must be true in the lit region outside the SB transition region and $\bar{R} \to \bar{T}$ must be true in the shadow region outside the SB transition region. Furthermore, the functional forms of $\bar{R}$ and $\bar{T}$ are assumed to be the same for cylindrical, spherical, or any other convex shape, as is true of the $\bar{R}$ and $\bar{T}$ dyads in the GTD solution.

(c) The uniform GTD solution for the electromagnetic case may also be simply expressed in terms of the corresponding scalar (or acoustic) soft and hard cases, respectively, as in the GTD solution [see Equations (5a), and (12b)].

Thus, the form of the uniform GTD solution for the total electric field, $\bar{E}$ may be expressed via the conjectures in (a) and (b) above, as:

$$\bar{E}(P_L) \sim \bar{E}^i(P_L) + \bar{E}^i(Q_R) \cdot \bar{\bar{R}} \sqrt{\frac{\rho_1^r \rho_2^r}{(\rho_1^r + s^r)(\rho_2^r + s^r)}}\; e^{-jks^r} \quad ; \quad \text{for } P_L \text{ in the } \underline{\text{lit}} \text{ region} \tag{19a}$$

$$\bar{E}(P_s) \sim \bar{E}^i(Q_1) \cdot \bar{\bar{T}} \sqrt{\frac{\rho_2^d}{s^d(\rho_2^d + s^d)}}\; e^{-jks^d} \quad ; \quad \text{for } P_s \text{ in the } \underline{\text{shadow}} \text{ region.} \tag{19b}$$

The incident ray field $\bar{E}^i$ is the same as in Equation (2) or (10). From conjecture (c) above, one may express $\bar{\bar{R}}$ and $\bar{\bar{T}}$ in terms of their corresponding acoustic soft and hard functions as:

$$\bar{\bar{R}} = R_s \, \hat{e}_\perp \, \hat{e}_\perp + R_h \, \hat{e}_\parallel^i \, \hat{e}_\parallel^r \quad , \tag{20}$$

$$\bar{\bar{T}} = T_s \, \hat{b}_1 \hat{b}_2 + T_h \, \hat{n}_1 \hat{n}_2 \quad . \tag{21}$$

The results in Equations (19a;b) together with the dyadics in Equations (20) and (21) are expressed in the same incident, reflected and surface diffracted ray coordinates as those employed in the GTD solution of Section II. The subscripts s and h in Equations (20) and (21) refer to the acoustic soft and hard cases, as before. From Equations (20) and (21), and conjecture (b) above, an obvious choice of $R_{\substack{s\\h}}$ and $T_{\substack{s\\h}}$ is directly available from the acoustic soft or hard solution of Equations (A-16a;b) in the Appendix. Thus,

$$R_{\substack{s\\h}} = - \left[\sqrt{\frac{-4}{\xi^L}} \, e^{-j(\xi^L)^3/12} \left\{ \frac{e^{-j\frac{\pi}{4}}}{2\sqrt{\pi}\xi^L} \left[1 - F(X^L) \right] + \hat{P}_{\substack{s\\h}}(\xi^L) \right\} \right] , \quad \text{for the } \underline{\text{lit}} \text{ region} \tag{22}$$

and

$$T_{\substack{s\\h}} = - \left[\sqrt{m(Q_1) m(Q_2)} \, \sqrt{\frac{2}{k}} \left\{ \frac{e^{-j\frac{\pi}{4}}}{2\sqrt{\pi}\xi^d} \left[1 - F(X^d) \right] + \hat{P}_{\substack{s\\h}}(\xi^d) \right\} \right] \sqrt{\frac{d\eta(Q_1)}{d\eta(Q_2)}} \, e^{-jkt} , \quad \text{for the } \underline{\text{shadow}} \text{ region.} \tag{23}$$

The various parameters occurring in Equations (22) and (23) are thus defined below as in Equations (A-11a) through (A-11ℓ) of the Appendix.

$$\xi^L = -2m(Q_R)\left[f(Q_R)\right]^{-1/3}\cos\theta^i ; \qquad f(Q_R) = 1 + \frac{\rho_g(Q_R)}{\rho_t(Q_R)}\cos^2\theta^i ; \qquad \xi^d = \int_{Q_1}^{Q_2} dt' \, \frac{m(t')}{\rho_g(t')} ; \tag{24a;24b;24c}$$

$$m(Q) = \left[\frac{k\rho_g(Q)}{2}\right]^{1/3} ; \qquad t = \int_{Q_1}^{Q_2} dt' ; \tag{24d;24e}$$

$$X^L = 2k\mathcal{L}^L \cos^2\theta^i ; \qquad X^d = \frac{k\,\mathcal{L}^d(\xi^d)^2}{2m(Q_1)m(Q_2)} . \tag{24f;24g}$$

For an electromagnetic spherical wave (or point source) type illumination, and for the field point in the far zone where $s^r \gg \rho^r_{1,2}$ and $s^d \gg \rho^d_2$ in Equations (19a;b) such that $\sqrt{\frac{\rho^r_1 \rho^r_2}{(\rho^r_1+s^r)(\rho^r_2+s^r)}} \approx \frac{\sqrt{\rho^r_1 \rho^r_2}}{s^r}$, and $\sqrt{\frac{\rho^d_2}{s^d(\rho^d_2+s^d)}} \approx \frac{\sqrt{\rho^d_2}}{s^d}$, the "distance" parameters $\mathcal{L}^L$ and $\mathcal{L}^d$ in Equations (24f;24g) are given for this special case by $\mathcal{L}^L = s^r$ and $\mathcal{L}^d = s^d$ as in Equations (A-16a;b). It is noted that s^r, s^d and ρ^d_2 appearing in Equations (19a;b) correspond to ℓ, s_3 and ρ_c in Equations (A-16a;b), respectively. Therefore, in order to complete the solution in Equations (19a;b) for the general case, one need only specify the parameters $\mathcal{L}^L$ and $\mathcal{L}^d$. To recapitulate, the general case deals with an arbitrary incident ray optical electromagnetic field, an arbitrary convex surface, and a near zone field point (for which the field point may be several wavelengths from the scattering surface, but yet not far in comparison with the characteristic dimensions of the scatterer). As mentioned previously in Section I, the plane, cylindrical, conical and spherical wavefronts are special cases of the arbitrary quadratic wavefront approximation implied in the ray optical description of the incident field. Recalling that the role of the $F(X^L)$ and $F(X^d)$ functions is to ensure the continuity of the total field at SB, one may then evaluate X^L and X^d appearing in X^L and X^d, respectively, by actually enforcing the continuity of the total field at SB. This procedure is exactly analogous to that employed previously by Kouyoumjian and Pathak [16] in their development of a uniform GTD solution for the diffraction of an arbitrary ray optical electromagnetic field by an edge in an otherwise smooth surface. Let P_{SB} denote a field point on SB. The continuity of the total field at SB requires that

$$\lim_{P_L \to P_{SB}} \overline{E}(P_L) = \lim_{P_s \to P_{SB}} \overline{E}(P_s) \quad , \tag{25}$$

in which $\overline{E}(P_L)$ and $\overline{E}(P_s)$ are given by Equations (19a) and (19b). Employing the limiting form of Equation (17) for the F function, and the definition given in Equation (18) for the $\hat{P}_{s \atop h}$ function, into Equations (22) and (23), allows one to write Equation (25) as:

$$\begin{pmatrix}\hat{b}_1\\ \hat{n}_1\end{pmatrix} \cdot \overline{E}^i(P_{SB}) - \begin{pmatrix}\hat{b}_1\\ \hat{n}_1\end{pmatrix} \cdot \overline{E}^i(Q_1)\left[\frac{\sqrt{L^L}}{2} + m(Q_1)\sqrt{\frac{2}{k}}\, e^{-j\frac{\pi}{4}} \begin{pmatrix}p^*(0)\\ q^*(0)\end{pmatrix}\right]\sqrt{\frac{1}{s}\left(\frac{\rho_2^r}{\rho_2^r+s}\right)}\, e^{-jks}$$

$$= - \begin{pmatrix}\hat{b}_1\\ \hat{n}_1\end{pmatrix} \cdot \overline{E}^i(Q_1)\left[-\frac{\sqrt{L^d}}{2} + m(Q_1)\sqrt{\frac{2}{k}}\, e^{-j\frac{\pi}{4}} \begin{pmatrix}p^*(0)\\ q^*(0)\end{pmatrix}\right]\sqrt{\frac{1}{s}\left(\frac{\rho_2^d}{\rho_2^d+s}\right)}\, e^{-jks},$$

$$\text{at the SB.} \tag{26}$$

With the distance from Q_1 to P_{SB} defined as s, one obtains.

$$s^r\Big|_{SB} = s \quad ; \qquad s^d\Big|_{SB} = s \quad . \tag{27a;27b}$$

It is noted that if $P_L \to P_{SB}$, then $\theta^i \to \pi/2$, $\xi^L \to 0$, $Q_R \to Q_1$, $\rho_1^r \to 0$ (see Equation (7a)), $\hat{e}_\parallel^i \to \hat{n}_1$, $\hat{e}_\parallel^r \to \hat{n}_1$, and $\hat{e}_\perp \to \hat{b}_1$. Likewise, if $P_s \to P_{SB}$, then $\xi^d \to 0$, $Q_2 \to Q_1$, $t \to 0$, $\hat{n}_2 \to \hat{n}_1$, and $\hat{b}_2 \to \hat{b}_1$. Furthermore, at SB, $\rho_2^r = \rho_2^d$. The functions $p^*(\delta)$ and $q^*(\delta)$ are continuous everywhere including $\delta=0$. Let the incident field be described by a diverging wavefront in the direction of propagation at Q_1 (i.e., at grazing); thus, one may write,

$$\begin{pmatrix} \hat{b}_1 \\ \hat{n}_i \end{pmatrix} \cdot \bar{E}^i(Q_1) = \begin{pmatrix} a_\perp(\bar{r}_0) \\ a_\parallel(\bar{r}_0) \end{pmatrix} \sqrt{\frac{\rho_1^i \rho_2^i}{(\rho_1^i+s_0)(\rho_2^i+s_0)}} \; e^{-jks_0} , \tag{28}$$

where s_0 denotes the distance s^i from some reference point at $\bar{r}_0$ to the point 0_1. The quantities $\bar{a}_\perp(\bar{r}_0)$ and $\bar{a}_\parallel(\bar{r}_0)$ which are the $\hat{b}_1$ and $\hat{n}_1$ directed amplitudes of $\bar{E}^i$ at the reference location $(\bar{r}_0)$ are assumed known. It follows from Equation (28) that

$$\begin{pmatrix} \hat{b}_1 \\ \hat{n}_1 \end{pmatrix} \cdot \bar{E}^i(P_{SB}) = \begin{pmatrix} a_\perp(\bar{r}_0) \\ a_\parallel(\bar{r}_0) \end{pmatrix} \sqrt{\frac{\rho_1^i \rho_2^i}{(\rho_1^i+[s_0+s])(\rho_2^i+[s_0+s])}} \; e^{-jk[s_0+s]} . \tag{29}$$

The incident wave caustic distances $\rho_{1,2}^i$ are measured from the reference point at $\bar{r}_0$ to the respective caustic locations. Incorporating Equations (28) and (29) into (26) yields

$$L^L\Big|_{SB} = L^d\Big|_{SB} = \frac{(\rho_1^i+s_0)(\rho_2^i+s_0)}{(\rho_1^i+[s_0+s])(\rho_2^i+[s_0+s])} \; \frac{s(\rho_2^r+s)}{\rho_2^r} \quad , \text{ at SB.} \tag{30}$$

Since the distance parameter is a slowly varying quantity near SB, and since (1-F) vanishes sufficiently rapidly as the field point moves far from SB; it is convenient to use the value in Equation (30) for L^L and L^d even away from SB. It is assumed of course in the present development (as pointed out in Section I), that the field point location and the caustics of the incident wavefront are not in the close vicinity of the surface, and that the field point itself is not in the neighborhood of any caustics associated with the incident and scattered rays. Furthermore, it is assumed that the amplitude of the incident ray optical field does not exhibit a rapid spatial variation in the vicinity of the points of reflection and diffraction on the surface. This completes the construction of the uniform GTD solution in Equations (19a;b) for a diverging wavefront.

If the incident wavefront is of the converging, or converging-diverging type, then the parameters $\ell^{L,d}$ in Equation (30) can become negative. It has not been investigated in detail how the general solution can be completed when $\ell^{L,d}$ becomes negative. However, if one of the principal directions of the incident wavefront coincides with one of the principal planes of the surface at grazing, then one can treat a converging or converging-diverging type wavefront for which $\ell^{L,d}<0$, by replacing $F(X^{L,d})$ with $F^*(|X^{L,d}|)$. The $*$ on $F^*(|X^{L,d}|)$ denotes the complex conjugate operator. The use of $F^*(|X^{L,d}|)$ when $\ell^{L,d}<0$ leads to a continuous total field at SB in this case, and it's use may be justified as in the edge diffraction problem [19] via an analytic continuation procedure to include negative values of $X^{L,d}$ (or $\ell^{L,d}$) while simultaneously satisfying the radiation condition for the scattered field.

Finally, exterior to the SB transition region, the uniform GTD result of Equations (19a;b) does indeed recover the ordinary GTD result of Equations (10) and (12a) as may be verified by employing the limiting forms of Equations (15) and (16a;b) into Equations (22) and (23).

It is noted that a solution for the SB transition region pertaining to the same general problem as the one considered here has also been given by G. James*; however, his solution which is presented without sufficient details is not uniform in that it does not properly reduce to the GTD solution exterior to the SB transition region. Furthermore, that solution employs a "pseudo" ray path for the reflected field in the lit region; such a path does not satisfy the generalized Fermat's principle. On the other hand, as is well known, the GO reflected ray path which is employed in this paper indeed satisfies the generalized Fermat's principle.

IV. DISCUSSION AND NUMERICAL RESULTS

A uniform GTD solution has been obtained for the problem of the scattering of a ray optical electromagnetic field by a smooth, perfectly-conducting convex surface as shown in Figure 1. This result is explicitly given in Equation (19a) for the lit region, and in Equation (19b) for the shadow region, together with the parameters in Equations (20) through (24g), and also Equation (30). While the behavior across only a single shadow boundary (SB) is discussed in this paper in connection with the open convex surface of Figure 1, the present theory can just as easily treat the scattering by a closed convex surface. Basically, one treats a closed convex surface via the uniform GTD in the same manner as one would via the ordinary GTD; thus, the only difference between the two approaches is that the $\bar{\bar{R}}$ and $\bar{\bar{T}}$ dyads in the GTD solution are replaced by the more general and more accurate $\bar{\bar{\mathcal{R}}}$ and $\bar{\bar{\mathcal{T}}}$ dyads in the uniform GTD solution. It is noted of course that the

---

*G.L. James, Geometrical Theory of Diffraction for Electromagnetic Waves, published by Peter Peregrinus Ltd., Southgate House, Stevenage, Herts. SG1 1HQ, England, 1976.

usual GTD solution fails within the shadow boundary transition regions; whereas, the uniform GTD solution does not. When a surface of revolution is illuminated by a plane wave which is incident along the axis of revolution of the surface, a caustic of the surface diffracted rays lies on this axis. The uniform GTD solution fails (as does the usual GTD solution) in the neighborhood of such a caustic. However, if the field point is in the near zone such that the caustic and the shadow boundary directions are widely separated, then one can employ the method of equivalent ring currents to evaluate the field in the neighborhood of such a caustic. The equivalent currents in this case are found indirectly from the uniform GTD solution. Such a procedure will be reported in a separate paper together with another approximate technique which would yield the field near caustics for the special case when the caustic and the shadow boundary directions tend to coincide. The latter special case arises when the field point is near the axis but in the far zone behind the surface of revolution. The other restrictions on the uniform GTD solution are mentioned at the end of both, Sections I and III, respectively.

It is interesting to note that the ξ^{L} of Equation (24a) may be approximated for convenience by -2 $m(Q_R)\cos\theta^i$ (upon arbitrarily setting $f^{-1/3}(Q_R)=1$) without affecting the accuracy of the solution. Furthermore, it is easily verified that the $L^{L,d}$ parameter of Equation (30) simplifies to give the following:

$$
\mathcal{L}^{L,d} = \begin{cases} \dfrac{s's}{s'+s} \ , & \text{for a 2-D cylindrical wave (i.e., line source), or an obliquely incident 3-D spherical wave (i.e., point source) illumination.} \\ s \ , & \text{for a plane wave illumination } (s'\to\infty). \end{cases} \qquad (31)
$$

In the above expression, s' denotes the distance from the source point to the point of grazing incidence at Q_1. For the cylindrical wave illumination s' and s are to be interpreted as the distances in the complete 2-D problem. With $\mathcal{L}^{L,d}$ as in Equation (31) for plane, cylindrical, or spherical wave illumination, it is easily verified that the uniform GTD result of Equations (19a;b) satisfies reciprocity. Finally, this uniform GTD solution is simple and accurate to use since it is given in terms of the F and $\hat{P}_{\substack{s\\h}}$ type functions which are tabulated. These important aspects of the present uniform GTD solution are illustrated below by applying it to several interesting problems.

Consider an infinitely long circular cylinder of radius (a) as shown in Figure 6a. The geometrical optics field for this geometry is shown in Figure 6b for an electric dipole (acoustic soft boundary condition) and in Figure 6c for a magnetic dipole (acoustic hard boundary condition) mounted parallel to the cylinder axis. As is well known, the geometrical optics field breaks down near the shadow boundaries. This is readily apparent in these two figures. Nevertheless, this solution has often been applied to obtain a result for the scattering from a cylinder. The uniform GTD solution presented in this paper, however, can be quickly and accurately computed. The uniform GTD result is compared with the geometrical optics result in Figures 6b and c. Obviously, a much more complete result for the problem

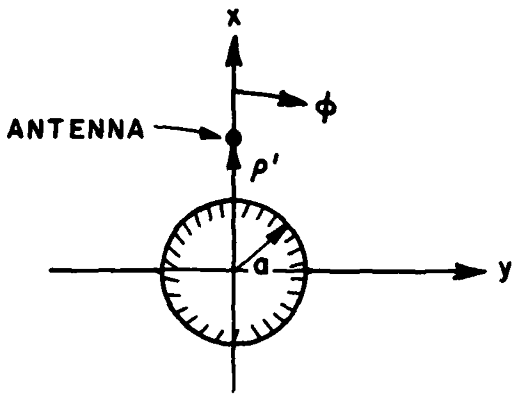

Figure 6a. Infinitely long circular cylinder.

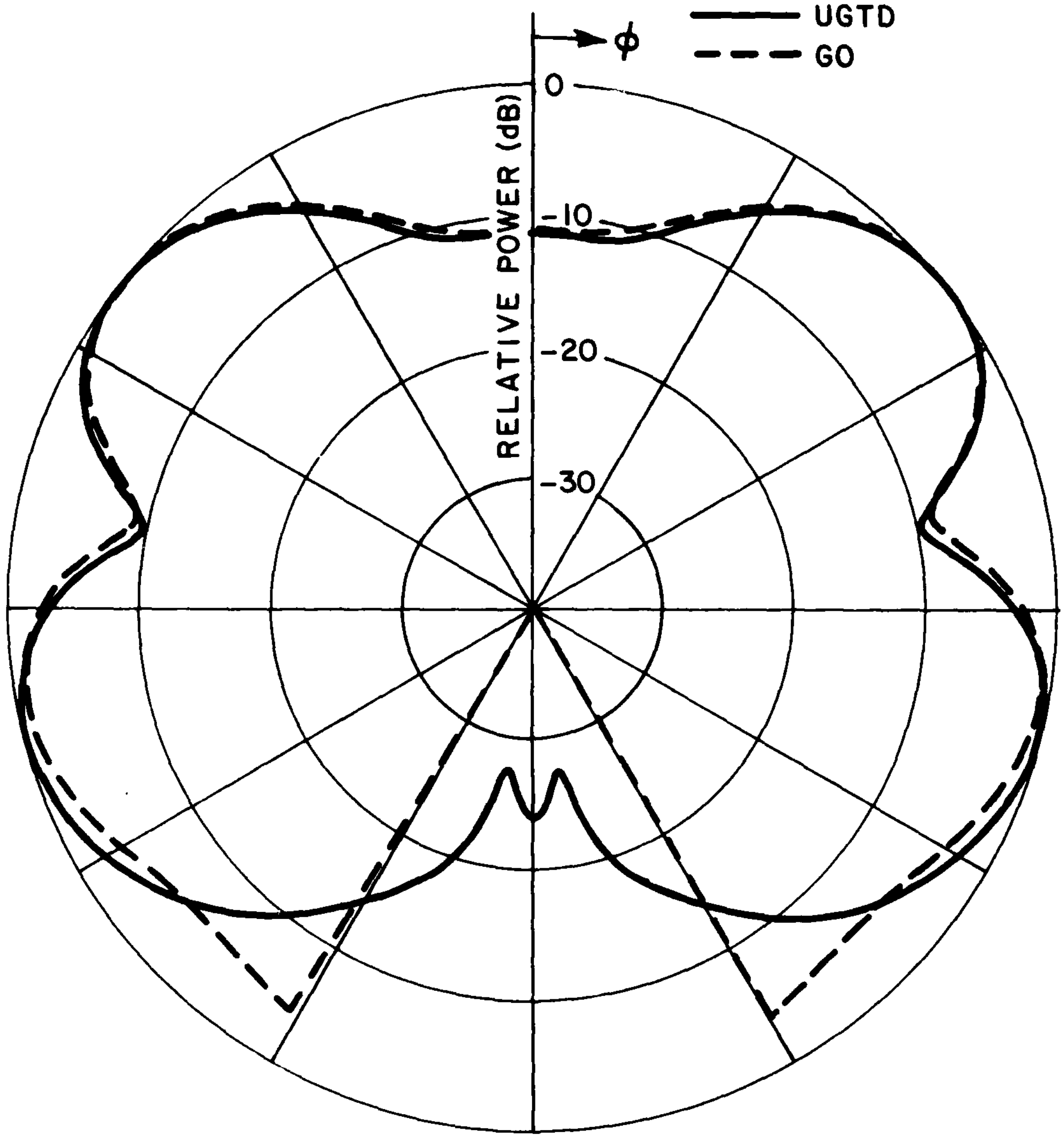

Figure 6b. Comparison of the geometrical optics and uniform geometrical theory of diffraction radiation patterns for an electric dipole in the presence of an infinitely long circular cylinder with $a = 1\lambda$ and $\rho' = 2\lambda$.

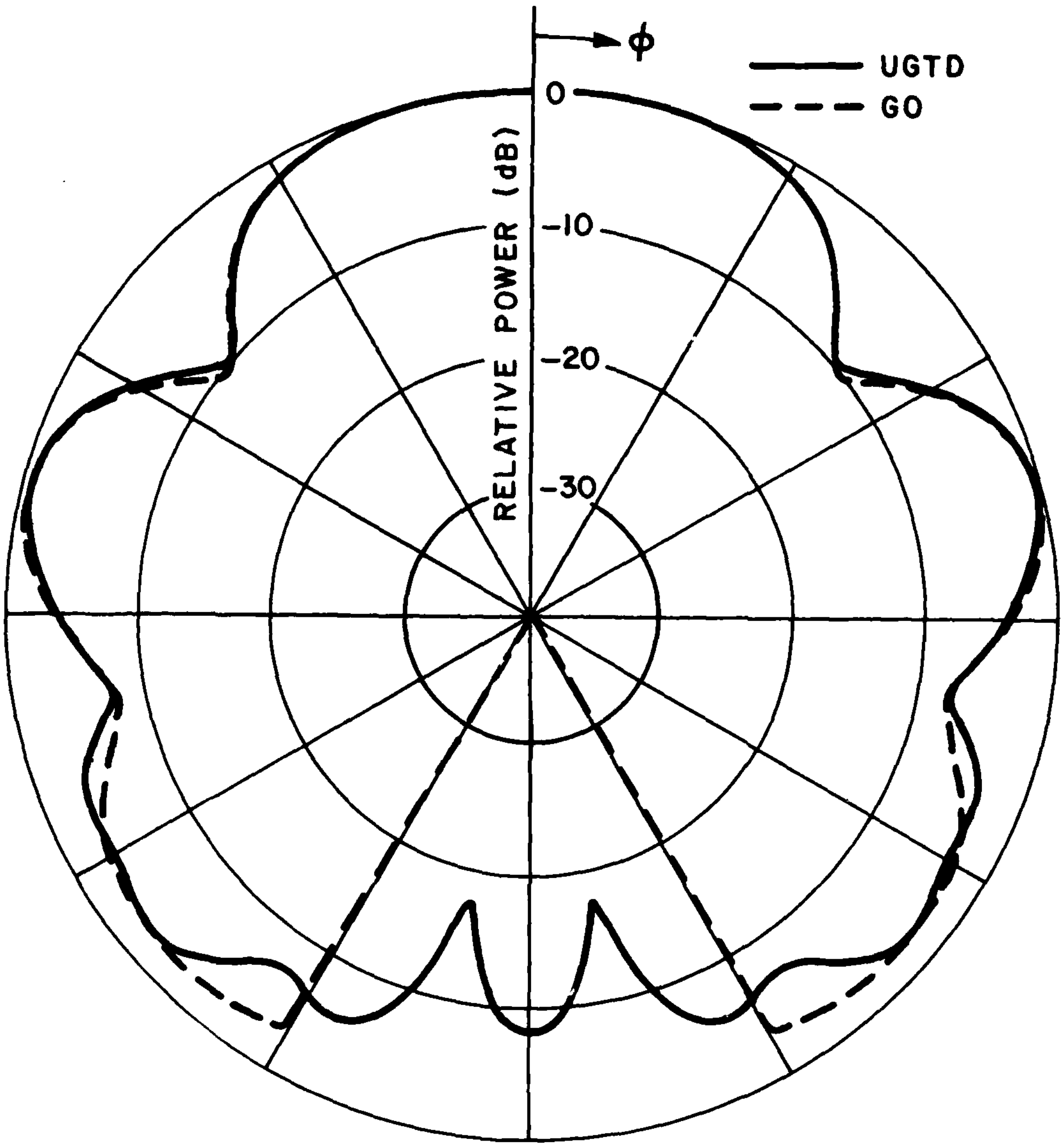

Figure 6c. Comparison of the geometrical optics and uniform geometrical theory of diffraction radiation patterns for a magnetic dipole in the presence of an infinitely long circular cylinder with $a = 1\lambda$ and $\rho' = 2\lambda$.

in Figure 6a is obtained using the uniform GTD presented here. The validity of this result is shown by comparing it with the exact eigenfunction solution. The exact and the uniform GTD results for the two polarizations are compared in Figure 7. The agreement is excellent and hence confirms the validity of the uniform GTD solution.

The next example is of an electric dipole in the presence of a finite circular cylinder, as illustrated in Figure 8a. Measurements have been made on this satellite shape by Bach [20] and are used for comparisons with the calculated results in Figure 8b. The pattern is taken in the x-y plane. The end caps of the cylinder do not have a large effect in this plane and, therefore, do not need to be included. Note that the dipole is aligned parallel to the x axis. This causes the cylinder to be illuminated by a slowly varying field. The measured and calculated results, however, are in good agreement within experimental accuracy.

An example of a magnetic dipole in the presence of an elliptic cylinder is considered next, as illustrated in Figure 9a. The pattern is a conic cut about the cylinder axis. The dipole is parallel to the cylinder axis. This could represent a slot mounted near an aircraft fuselage, engine, or store. The calculated result is compared against a result obtained from a moment method solution* in Figure 9b. The agreement is very good, again, verifying the validity of the present solution.

---

*This solution has been kindly furnished by Dr. N. Wang.

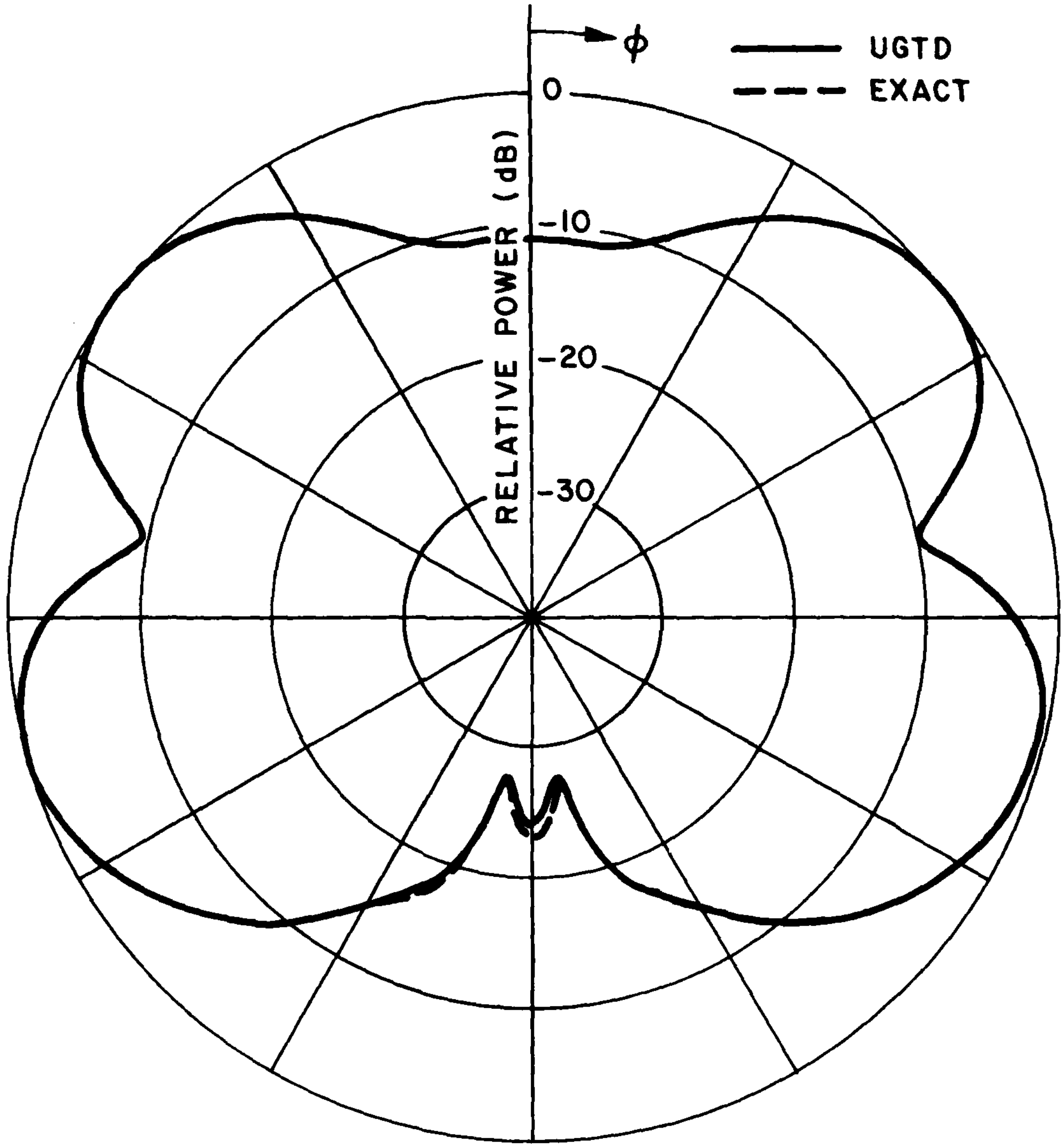

Figure 7a. Comparison of the exact eigenfunction and uniform geometrical theory of diffraction radiation patterns for an electric dipole in the presence of an infinitely long circular cylinder with $a = 1\lambda$ and $\rho' = 2\lambda$.

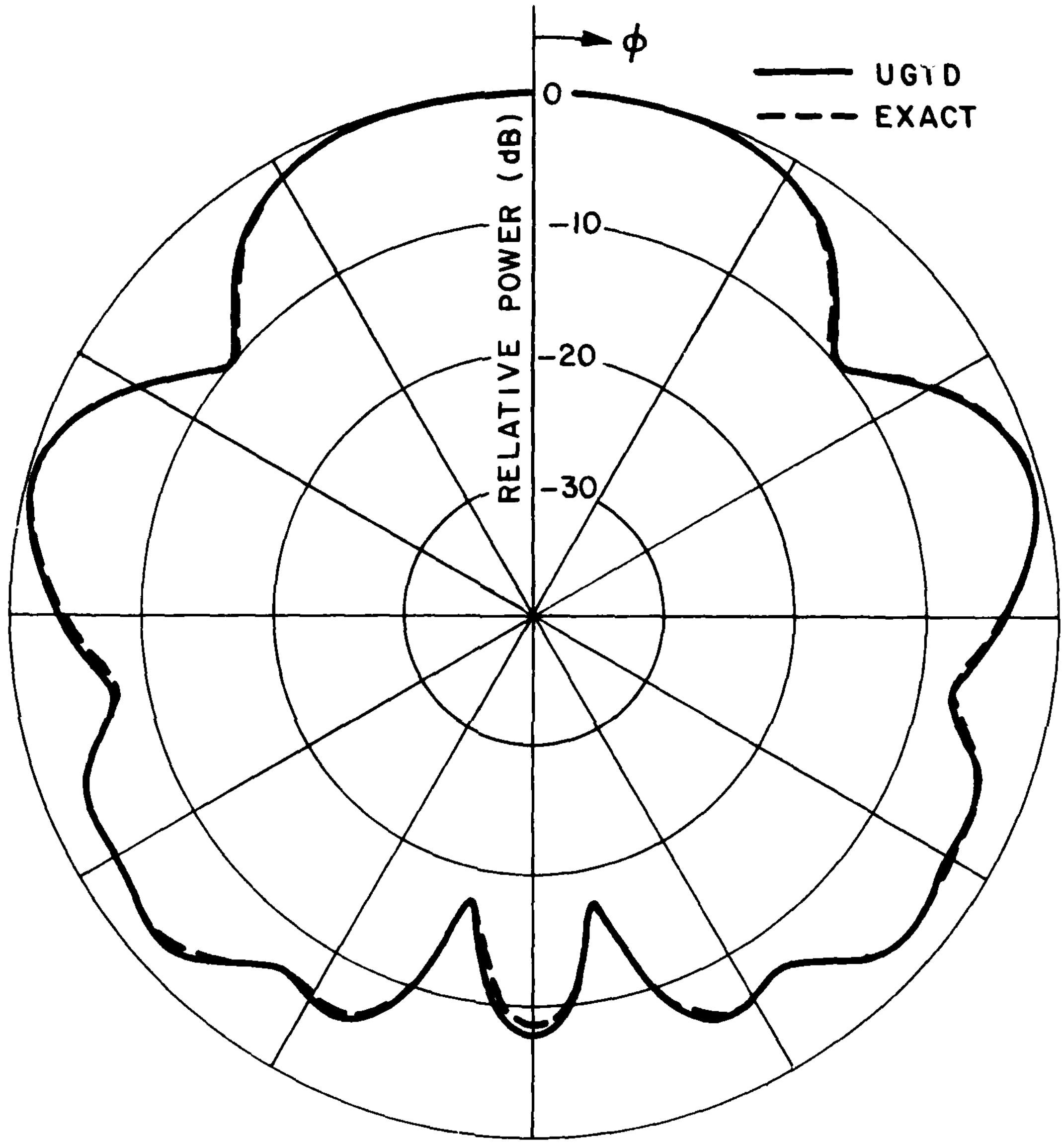

Figure 7b. Comparison of the exact eigenfunction and uniform geometrical theory of diffraction radiation pattern for a magnetic dipole in the presence of an infinitely long circular cylinder with $a = 1\lambda$ and $\rho' = 2\lambda$.

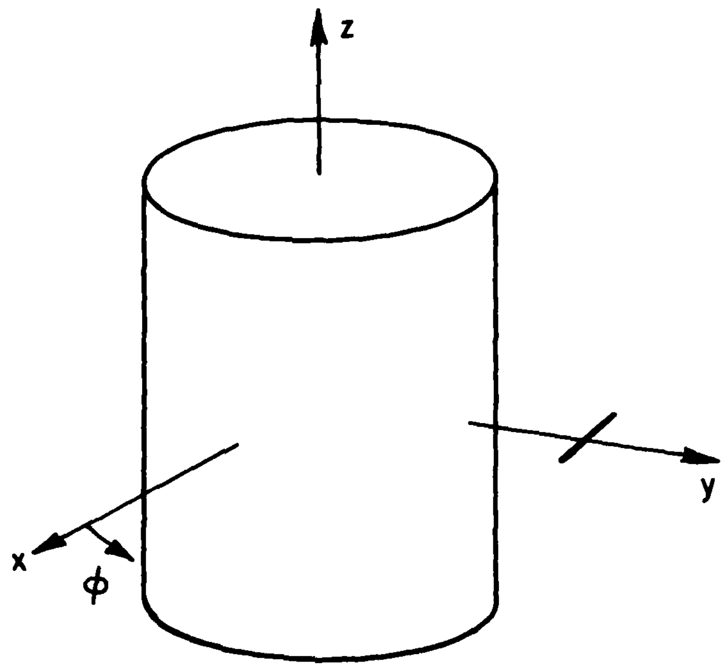

Figure 8a. Geometry of an electric dipole situated 19 cm from the center of a finite circular cylinder 10 cm in radius and 22 cm long.

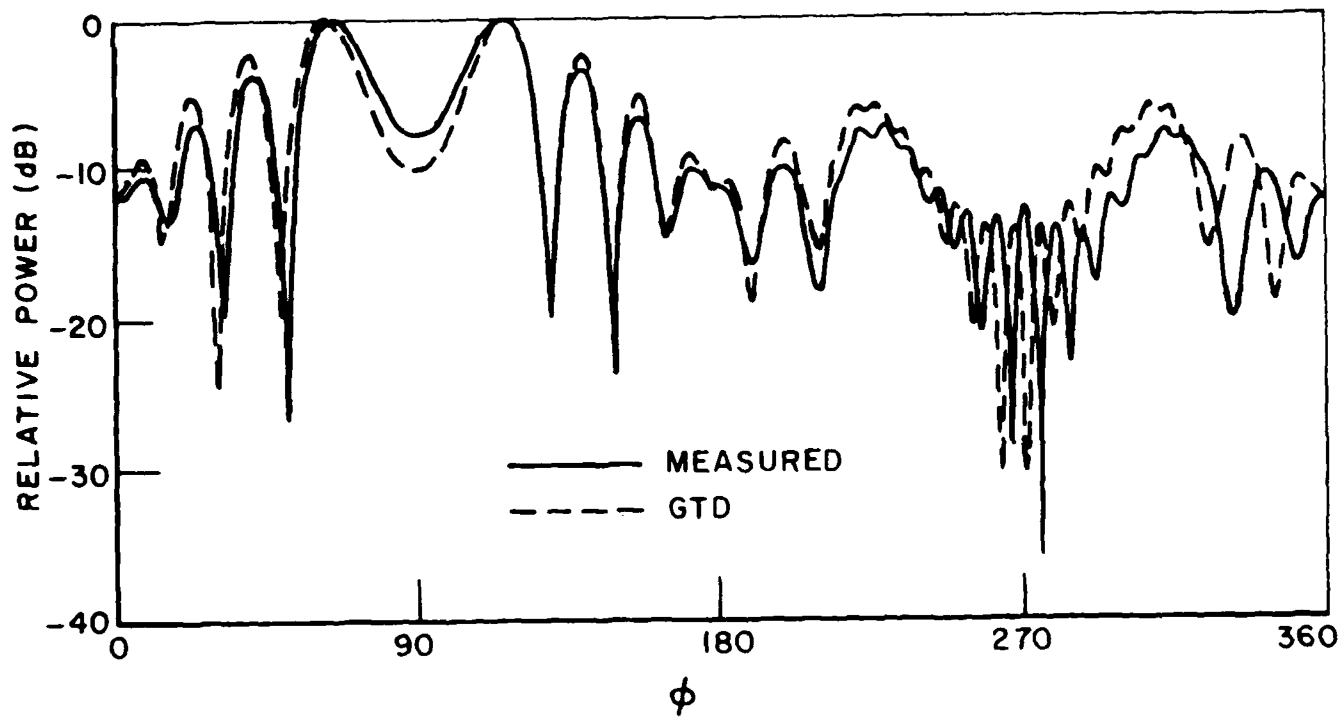

Figure 8b. Comparison of the measured (Bach) and calculated E_ϕ radiation pattern for an electric dipole on the y axis parallel to the x axis in the presence of a finite circular cylinder with the pattern taken in x-y plane.

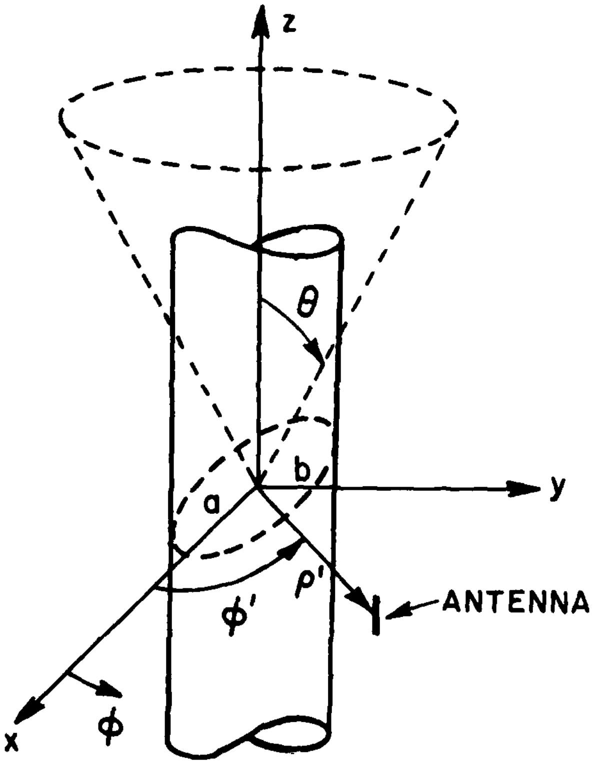

Figure 9a. Geometry for a magnetic dipole situated parallel to the axis of an infinitely long circular cylinder.

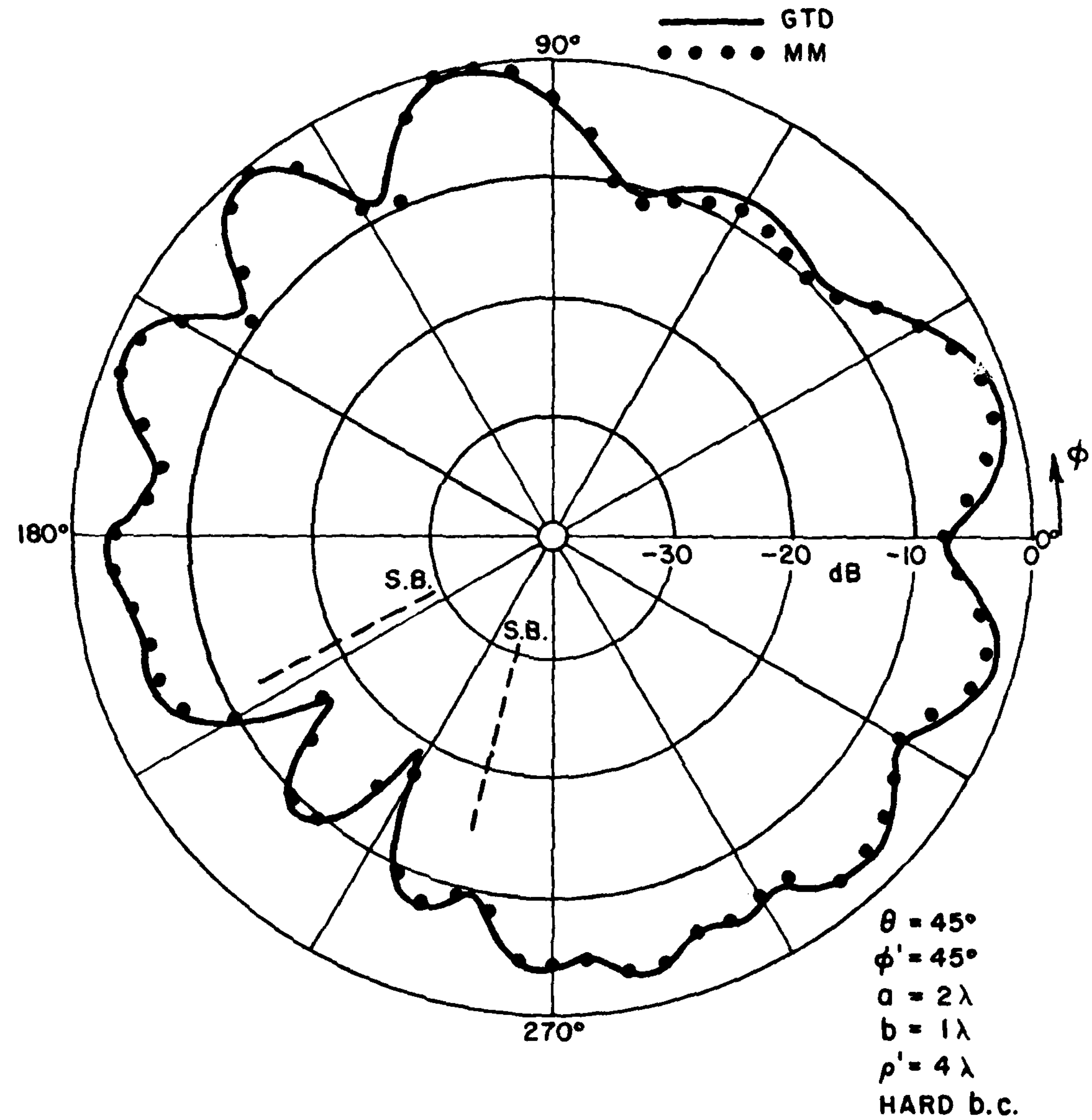

Figure 9b. Comparison of a moment method and uniform geometrical theory of diffraction radiation pattern for a magnetic dipole in the presence of an infinitely long circular cylinder. The pattern is a conic cut about the cylinder aixs.

In order to validate this solution in terms of a more complex surface consider the circular cone configuration illustrated in Figure 10. A half-wave dipole is located in the near zone of the cone, and the near zone field is measured as the receiver moves azimuthly around the axis of the cone. Both a vertical and horizontal dipole are treated with the resulting patterns shown in Figures 11a and 11b, respectively. In each case the calculated and measured results are in good agreement. Note that the receiver polarization was aligned with that of the transmitter in both cases.

The last example is used to show a cylinder being illuminated by a complex wavefront that can be represented in terms of an astigmatic tube of rays. The source of the astigmatic tube of rays or the quadratic ray pencil which impinges on the cylinder is the edge diffracted field of a plate mounted on the cylinder such that the cylinder is not in the shadow boundary transition region of the edge diffracted fields. The geometry used is illustrated in Figure 12. The antenna is a slot mounted parallel to the cylinder axis in the center of the plate. The calculated and measured results for this configuration are shown in Figure 12. There is good agreement between measured and calculated results, thus confirming the validity of the uniform GTD solution for a cylinder illuminated by a more general wavefront.

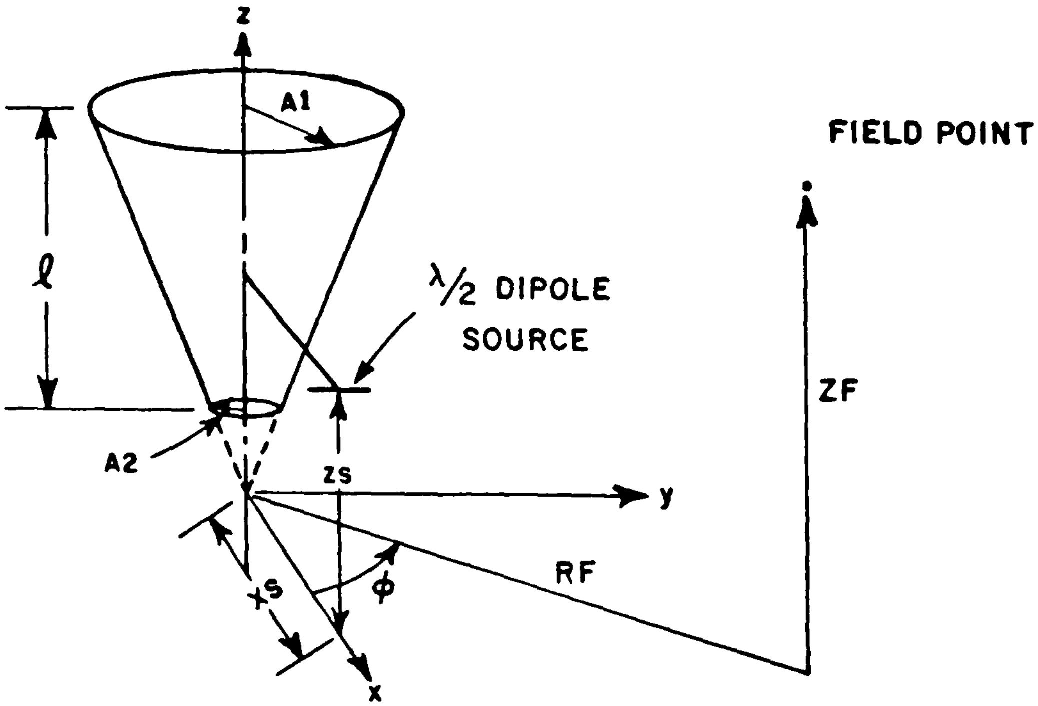

Figure 10. Geometry for the circular cone.

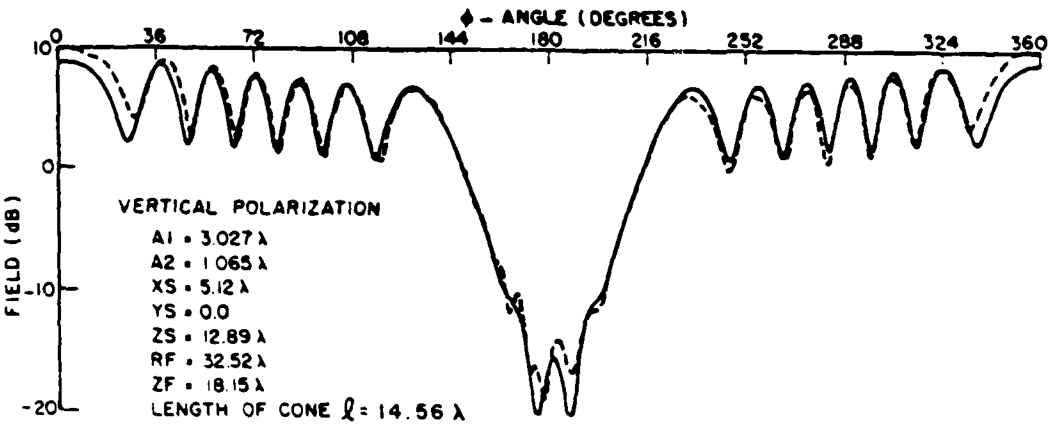

Figure 11a. Comparison of measured (dashed curve) and calculated (solid curve) radiation patterns for an electric dipole mounted parallel to the z axis of a circular cone.

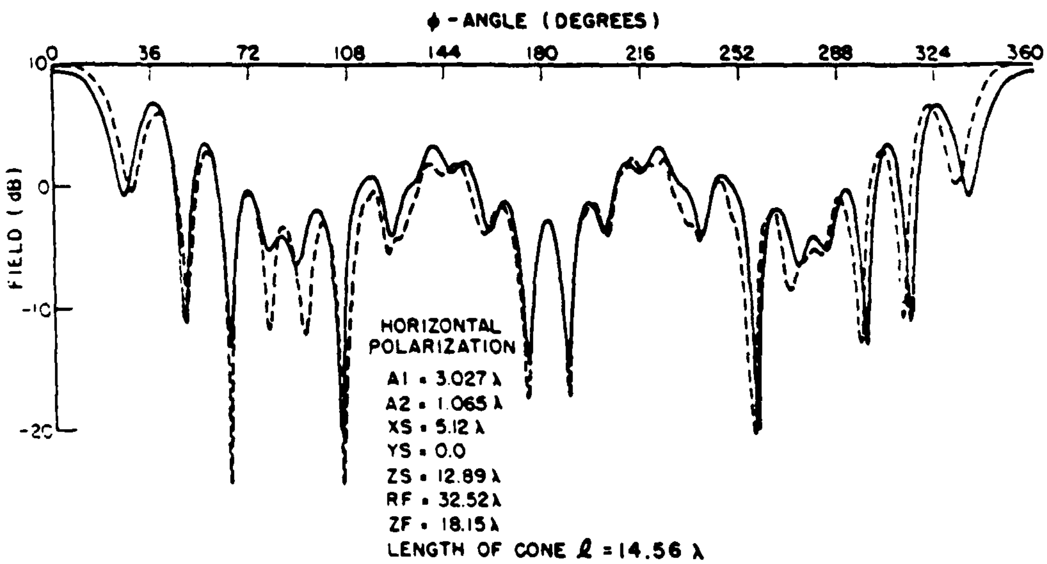

Figure 11b. Comparison of measured (dashed curve) and calculated (solid curve) radiation patterns for an electric dipole mounted paralle to the y axis of a circular cone.

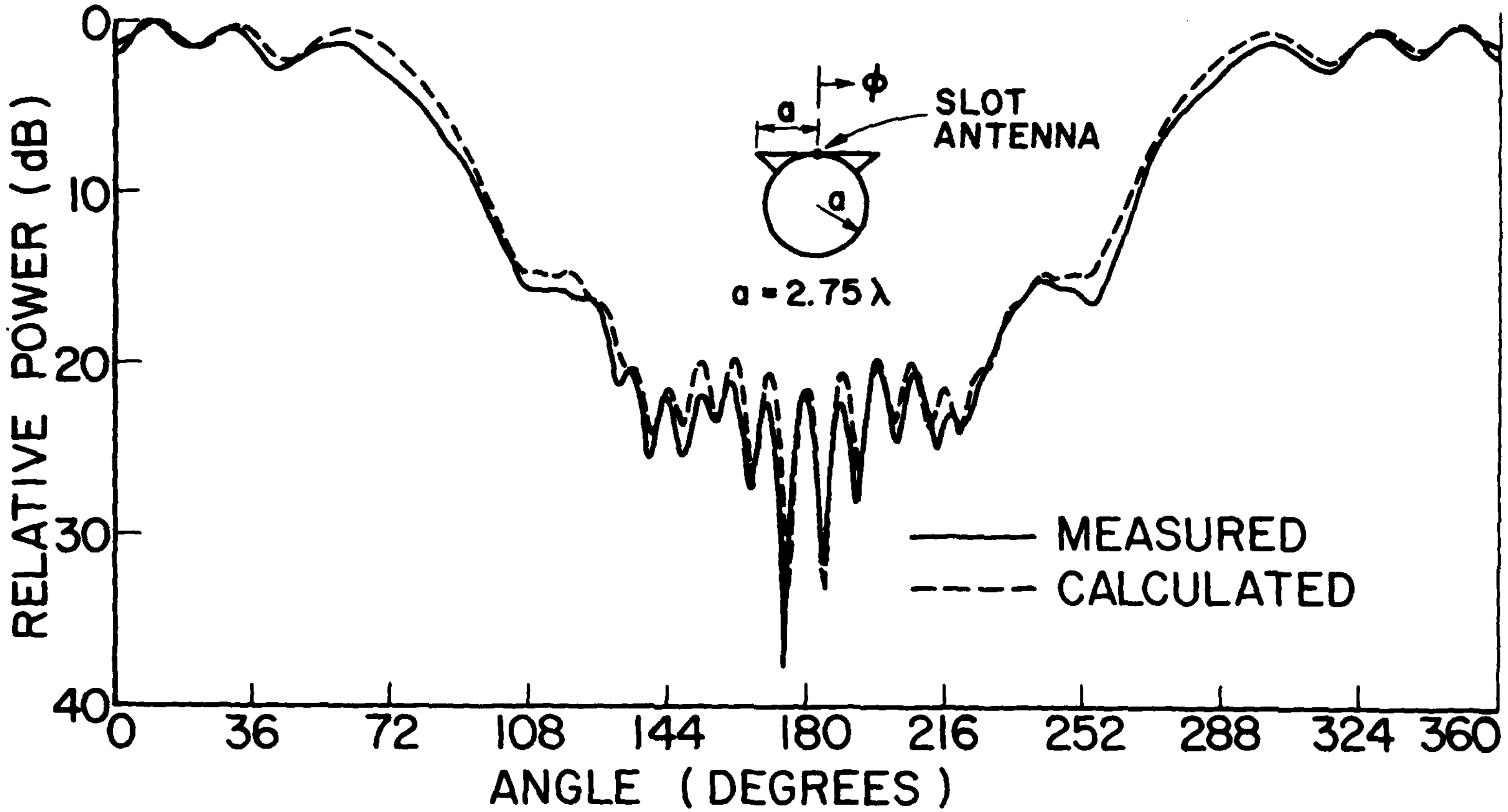

Figure 12. Comparison of measured and calculated radiation patterns for a slot mounted in a plate-cylinder configuration with the slot parallel to the cylinder axis.

REFERENCES

1. J. B. Keller, "Geometrical Theory of Diffraction, J. Opt. Soc. Am., Vol. 52, No. 2, pp. 116-130, 1962.

2. J. B. Keller, "Diffraction by a Convex Cylinder," Trans. I.R.E., Vol. AP-24, pp. 312-321, 1956.

3. B. R. Levy and J. B. Keller, "Diffraction by a Smooth Object," Comm. Pure and Appl. Math., Vol. 12, pp. 159-209, 1959.

4. P. H. Pathak, "An Asymptotic Analysis of the Scattering of Plane Waves by a Smooth Convex Cylinder," paper to appear in J. Radio Science. (Also The Ohio State University ElectroScience Laboratory Tech. Report 784583-3, March 1978).

5. P. H. Pathak, R. J. Marhefka and W. D. Burnside, "High Frequency Scattering by Curved Surfaces," The Ohio State University ElectroScience Laboratory Tech. Report 3390-5, June 1974.

6. V. A. Fock, "Diffraction, Refraction and Reflection of Waves: Thirteen Papers," Air Force Cambridge Research Center Report AFCRC-TN-57-102, (AD 117276), 1957. Also V. A. Fock, <u>Electromagnetic Diffraction and Propagation Problems</u>, Pergamon Press, 1965.

7. V. A. Fock, "Fresnel Diffraction from Convex Bodies," Uspekii Fizicheskikh Nauk., Vol. 43, pp. 587-599, 1951. (Also in Reference [6]).

8. J. R. Wait and A. M. Conda, "Diffraction of Electromagnetic Waves by Smooth Obstacles for Grazing Angles," Jour. of Res., N.B.S., Vol. 63D, No. 2, pp. 181-197, 1959.

9. N. A. Logan, "General Research in Diffraction Theory," Vol. I, LMSD-288087; and Vol. II, LMSD-288088, Missiles and Space Division, Lockheed Aircraft Corp., 1959.

10. N. A. Logan and K. S. Yee, <u>Electromagnetic Waves</u>, Edited by R. E. Langer, Univ. of Wisconsin Press, 1962.

11. V. I. Ivanov, "Uniform Asymptotic Behavior of the Field Produced by a Plane Wave Reflection at a Convex Cylinder," U.S.S.R. Journal of Computational Math. and Math. Phys. (Translated from Zl. Vychisl, Mat. Mat. Fiz.), Vol. 2, p. 216, 1971.

12. R. K. Luneberg, Mathematical Theory of Optics, Notes issued by Brown University, 1964.

13. M. Kline, "An Asymptotic Solution of Maxwell's Equation," Comm. Pure and Appl. Math., Vol. 4, pp. 225-263, 1951.

14. S. W. Lee, "Geometrical Optics," University of Illinois Electromagnetics Laboratory Tech. Report 78-2, 1978.

15. R. G. Kouyoumjian, "The Geometrical Theory of Diffraction and Its Application," Ch. 6 of Numerical and Asymptotic Techniques in Electro-Magnetics (Ed. R. Mittra), Springer-Verlag, Berlin, 1975.

16. R. G. Kouyoumjian and P. H. Pathak, "A Uniform Geometrical Theory of Diffraction for an Edge in a Perfectly-Conducting Surface," Proc. IEEE, Vol. 62, pp. 1448-1461, 1974.

17. D. R. Voltmer, "Diffraction by Doubly Curved Convex Surfaces," Ph.D. Dissertation, Ohio State University, Columbus, Ohio 1970.

18. M. Abramowitz and I. A. Stegun, Handbook of Mathematical Functions, National Bureau of Standards Publication, 1970.

19. J. D. Cashman, R. G. Kouyoumjian and P. H. Pathak, comments on "A Uniform Theory of Diffraction for an Edge in a Perfectly-Conducting Surface," IEEE Trans., AP-25, No. 3, pp. 447-451, 1977. (Also P. H. Pathak and R. G. Kouyoumjian, "An Expression for the Uniform Edge Diffraction Coefficient When There is a Caustic on the Shadow Boundary," paper presented at the 1976 USNC-URSI meeting in Amherst, Mass.).

20. H. Bach, "Pattern Measurements of HF Satellite Mounted Antennas," Electromagnetic Institute, Technical University of Denmark, R154, 1976.

APPENDIX

FAR ZONE FIELDS OF A SCALAR POINT SOURCE RADIATING IN THE PRESENCE OF A SMOOTH CONVEX CYLINDER

An approximate uniform asymptotic result for the field ($\tilde{u}_2$) exterior to a smooth convex cylinder illuminated by an incident plane wave ($\tilde{u}_2^i$) is presented in Equations (45a) and (44a) of [4]. It is repeated here as follows:

$$\tilde{u}_2(\tilde{P}) \sim \tilde{u}_2^i(\tilde{P}) + \tilde{u}_2^i(Q_R)\left[-\sqrt{\frac{-4}{\xi'}}\, e^{-j\frac{(\xi')^3}{12}} \left\{\frac{e^{-j\frac{\pi}{4}}}{2\sqrt{\pi}\,\xi'}\left[1-F(X')\right] + \hat{P}_{\substack{s\\h}}(\xi')\right\}\right] \sqrt{\frac{\tilde{\rho}^r}{\tilde{\rho}^r+\ell_2}}\, e^{-jk\ell_2};$$

for $\tilde{P}$ in the lit region. (A-1a)

$$\tilde{u}_2(\tilde{P}) \sim \tilde{u}_2^i(Q_a)\left[-\sqrt{m(Q_a)m(Q_b)}\left\{e^{-jkt_2}\sqrt{\frac{2}{k}}\; \frac{e^{-j\frac{\pi}{4}}}{2\sqrt{\pi}\,\xi}\left[1-F(X)\right] + \hat{P}_{\substack{s\\h}}(\xi)\right\}\right] \frac{e^{-jks_2}}{\sqrt{s_2}};$$

for $\tilde{P}$ in the shadow region. (A-1b)

The subscripts "s" and "h" refer to the acoustic soft and hard cases, respectively; whereas, the subscript 2 refers to the two-dimensional (2-D) nature of the problem. The points $\tilde{P}$, Q_R, Q_a and Q_b in Equations (A-1a;b) are illustrated in Figure A-1 for the case when $\theta_o = \pi/2$; i.e., for "normal incidence". Also, the parameters for the lit region are given by

$$\xi' = -2m(Q_R)\cos\theta^i \quad ; \qquad \tilde{\rho}^r = \frac{\rho_g(Q_R)\cos\theta^i}{2} \quad ; \qquad \text{(A-2a;A-2b)}$$

$$m(Q_R) = \left[\frac{k\rho_g(Q_R)}{2}\right]^{1/3} , \tag{A-2c}$$

in which $\rho_g(Q_R)$ is the radius of curvature of the surface at Q_R, and

$$X' = 2k\ell_2\cos^2\theta^i \quad . \tag{A-2d}$$

The shadow region parameters are given by

$$\xi = \int_{Q_a}^{Q_b} \frac{m(t')}{\rho_g(t')} dt' \quad ; \qquad t_2 = \int_{Q_a}^{Q_b} dt' \quad ; \tag{A-2e;A-2f}$$

$$X = \frac{ks_2 \ \xi^2}{[2m(Q_a)m(Q_b)]} \quad ; \qquad m(t') = \left[\frac{k\rho_g(t')}{2}\right]^{1/3} \quad . \tag{A-2g;A-2h}$$

It is noted from Figure A-1 that $s_2 = s_3$ (for $\theta_o = \pi/2$); $\ell_2 = \ell_3$(for $\theta_o = \pi/2$). The functions F and $\hat{P}$ are defined by [4]

$$F(\delta) = 2j\sqrt{\delta}\, e^{j\delta} \int_{\sqrt{\delta}}^{\infty} d\tau\, e^{-j\tau^2} \quad ; \quad \text{for } \delta>0 \ \ (\text{for } \delta<0, \text{ see Section III of text}). \tag{A-3}$$

$$\hat{P}_{\substack{s\\h}}(\sigma) = \frac{e^{-j\frac{\pi}{4}}}{\sqrt{\pi}} \int_{-\infty}^{\infty} d\tau\, \frac{\tilde{Q}V(\tau)}{\tilde{Q}W_2(\tau)}\, e^{-j\sigma\tau} \quad ; \qquad \tilde{Q} = \begin{cases} 1, & \text{for acoustic soft case} \\ \frac{\partial}{\partial\tau}, & \text{for acoustic hard case.} \end{cases} \tag{A-4}$$

The σ in (A-4) is positive in the shadow region; whereas, it is negative in the lit region. The shadow boundary occurs at σ=0. The Fock type Airy functions $V(\tau)$ and $W_2(\tau)$ are defined in [9], such that

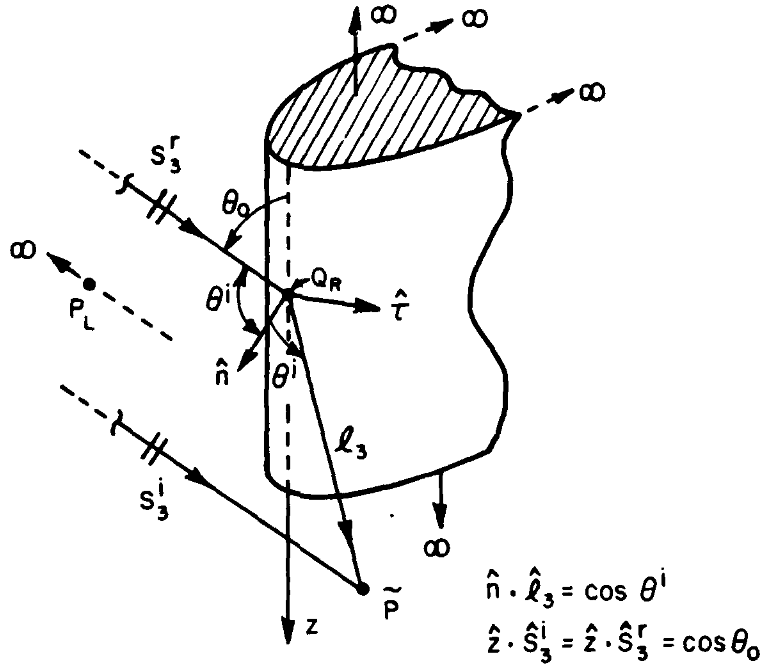

(a) INCIDENT AND REFLECTED RAY SYSTEM FOR THE FIELD POINT $\tilde{P}$ IN THE LIT ZONE

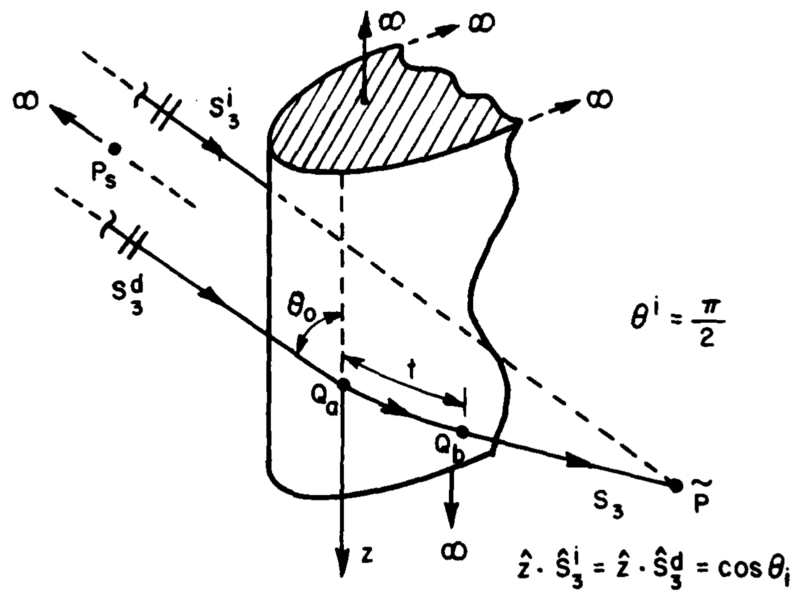

(b) SURFACE DIFFRACTED RAY PATH FOR THE FIELD POINT $\tilde{P}$ IN THE SHADOW ZONE

Figure A-I. Ray paths associated with the problem of scattering of an obliquely incident plane wave by a smooth convex cylinder.

$$2j\,V(\tau) = W_1(\tau) - W_2(\tau); \qquad W_{\substack{1\\2}}(\tau) = \frac{1}{\sqrt{\pi}} \int_{\Gamma_{\substack{1\\2}}} dt\, e^{\tau t - t^3/3} \, . \qquad \text{(A-5a;A-5b)}$$

The contour of integration Γ_1 runs from $\infty\, e^{-j(2\pi/3)}$ to ∞, and Γ_2 is the complex conjugate of Γ_1. The functions $F(\delta)$, $p^*(\sigma)$, and $q^*(\sigma)$ are plotted in [4]; it is noted that the functions $p^*(\sigma)$ and $q^*(\sigma)$ are simply related to $\hat{P}_s(\sigma)$ and $\hat{P}_h(\sigma)$, respectively, via the relations given in Equation (18) of Section III.

A solution to the three-dimensional (3-D) problem of the scattering of an obliquely incident plane wave by a smooth convex cylinder as in Figure A-1 is directly obtained from the solution in Equations (A-1a;b) for the 2-D normal incidence plane wave case via the method of separation of variables.

Let $\tilde{u}_3$ represent the total exterior field for the 3-D case, with the subscript "3" being employed to distinguish the 3-D nature of the problem. Then, $\tilde{u}_3$ satisfies the scalar wave equation,

$$(\nabla^2 + k^2)\,\tilde{u}_3 = 0. \qquad \text{(A-6)}$$

This obliquely incident plane wave field u_3^i may be expressed in the form

$$\tilde{u}_3^i = \tilde{u}_2^i(k_t)\, e^{-jk_z z} \quad ; \quad \begin{Bmatrix} k_z = k\cos\theta_o \\ k_t = k\sin\theta_o \end{Bmatrix} \qquad \text{(A7)}$$

where $\tilde{u}_2^i(k_t)$ has the same spatial dependence as $\tilde{u}_2^i$ in the 2-D result of Equations (A-1a;b) except that the "k" in those equations is now replaced by "k_t". Thus, $u_2^i(k_t)$ is the component of the incident field which propagates transverse to z with a wavenumber k_t. One notes that θ_o is the angle between the incident ray direction and the z-axis as in Figure A-1, where the z-axis is parallel to the generator of the cylinder. The scattered field can also be split up as in Equation (A-7). Consequently, one may write

$$\tilde{u}_3 = \tilde{u}_2(k_t)\, e^{-jk_z z} \quad , \tag{A-8}$$

where

$$(\nabla_t^2 + k_t^2)\tilde{u}_2 = 0 \quad ; \quad \left\{\nabla_t^2 = \nabla^2 - \frac{\partial^2}{\partial z^2}\right\} , \tag{A-9}$$

and $\tilde{u}_2$ or $\tilde{u}_2(k_t)$ is the same as in Equations (A-1a;b) with the "k" in those equations replaced by "k_t". Thus, $\tilde{u}_3$ is obtained via Equations (A-1a;b), (A-7) and (A-8) as

$$\tilde{u}_3(\bar{P}) \sim \tilde{u}_3^i(\bar{P}) + \tilde{u}_3^i(Q_R)\left[-\sqrt{\frac{-4}{\xi^L}}\, e^{-j(\xi^L)^3/12}\left\{\frac{e^{-j\frac{\pi}{4}}}{2\sqrt{\pi}\,\xi^L}\left[1-F(X^L)\right] + \hat{P}_{\substack{s\\h}}(\xi^L)\right\}\right]\sqrt{\frac{\tilde{\rho}_t^r}{\tilde{\rho}_t^r + \ell_3\sin\theta_o}}$$

$$e^{-jk_t\ell_3\sin\theta_o - jk_z z} \quad ;$$

for $\bar{P}$ in the lit region. (A-10a)

$$\tilde{u}_3(\bar{P}) \sim \tilde{u}_3^i(Q_a)\left[-\sqrt{m(Q_a)m(Q_b)}\, e^{-jk_t t_3\sin\theta_o}\sqrt{\frac{2}{k_t}}\left\{\frac{e^{-j\frac{\pi}{4}}}{2\sqrt{\pi}\,\xi^d}\left[1-F(X^d)\right] + \hat{P}_{\substack{s\\h}}(\xi^d)\right\}\right]$$

$$\frac{e^{-jk_t s_3\sin\theta_o - jk_z z}}{\sqrt{s_3\sin\theta_o}} \quad ;$$

for $\bar{P}$ in the shadow region.

(A-10b)

In obtaining Equation (A-10a) it is assumed for the sake of convenience that the origin of the z axis is located at the point of reflection, Q_R; whereas, in Equation (A-10b) it is assumed that the origin is at the point of grazing incidence, Q_a. This choice of the origin simply implies that the axial (z) separation between the points Q_R or Q_a, and the field point is the distance "z". Thus, $z=\ell_3\cos\theta_o$ in Equation (A-10a) for the lit zone; whereas, $z=s_3\cos\theta_o$ in Equation (A-15b) for the shadow zone. It is easily verified that, the parameters for the lit zone are

$$\xi^L = -2m(Q_R)f^{-1/3}\cos\theta^i; \qquad f=1+\frac{\rho_g}{\rho_{tn}}\cos^2\theta^i; \qquad \rho_t^r = \frac{\rho_\tau\cos\theta^i}{2\sin\theta_o} \;;$$

(A-11a;A-11b;A-11c)

$$X^L \simeq 2k_t(\ell_3\sin\theta_o)\frac{\cos^2\theta^i}{\sin^2\theta_o} = 2k\ell_3\cos^2\theta^i; \quad \rho_g^{-1} = \rho_\tau^{-1}\sin^2\omega_o + \rho_z^{-1}\cos^2\omega_o;$$

(A-11d;A-11e)

$$\rho_{tn}^{-1} = \rho_\tau^{-1}\cos^2\omega_o + \rho_z^{-1}\sin^2\omega_o; \qquad \hat{U}_2 = \hat{z}; \qquad \hat{U}_1 = \hat{U}_2 \times \hat{n}.$$

(A-11f;A-11g;A-11h)

The angle of incidence (θ^i) is defined as usual by $\hat{\ell}_3.\hat{n} = -\hat{s}^{i,r}.\hat{n} = \cos\theta^i$. The angle ($\omega_o$) is shown in Figure 4, and ρ_z and ρ_τ are the principal radii of curvatures of the surface along the $\hat{U}_2$ and $\hat{U}_1$ directions, respectively. In the case of a cylindrical surface, $\rho_z\rightarrow\infty$. The parameters ρ_g and ρ_{tn} are the surface radii of curvatures in the $(\hat{n},\hat{t})$ and $(\hat{n},\hat{b})$ planes, respectively, where the unit vectors $\hat{t}$, $\hat{n}$, $\hat{b}$ are shown in Figure 4a. It is noted that the definitions of $m(Q_R)$ and $\tilde{\rho}^r$ are the same as in Equations (A-2b) and (A-2c), respectively, except that $\rho_g(Q_R)$ in Equation (A-11e) has the same value as $\rho_g(Q_R)$ in Equation (A-2b) only for $\theta_o = \pi/2$ (when $k_z=0$ and $k_t=k$); otherwise, $\rho_g(Q_R)$ of Equation (A-2b) is really ρ_τ appearing in Equation (A-11e).

Furthermore, $\ell_2 = \ell_3 \sin\theta_o$. Likewise, the parameters in Equation (A-10b) for the shadow region are given by

$$\xi^d = \int_{Q_a}^{Q_b} \frac{m(t')}{\rho_g(t')}\, dt' \ ; \qquad t_3 = \int_{Q_a}^{Q_b} dt' \ ; \qquad X^d = \frac{ks_3(\xi^d)^2}{2m(Q_a)m(Q_b)} \ .$$

(A-11i;A-11j;A-11k)

The function m(t') is defined as in Equation (A-2h) with

$$\rho_g^{-1}(t') = \rho_\tau^{-1} \sin^2\theta_o + \rho_z^{-1}\cos^2\theta_o . \qquad \text{(A-11}\ell\text{)}$$

It is noted that $\rho_g(t')$ in Equations (A-2e;A-2h) for the normal incidence case ($\theta_o = \pi/2$) is identical to ρ_τ in Equation (A-11ℓ). *It is also noted* that $t_2 = t_3\sin\theta_o$. Thus, Equations (A-10a;b) become:

$$\tilde{u}_3(\tilde{P}) \sim \tilde{u}_3^i(\tilde{P}) + \tilde{u}_3^i(Q_R)\left[-\sqrt{\frac{-4}{\xi^L}}\, e^{-j(\xi^L)^3/12}\left\{\frac{e^{-j\frac{\pi}{4}}}{2\sqrt{\pi}\,\xi^L}\left[1-F(X^L)\right] + \hat{P}_{\substack{s\\h}}(\xi^L)\right\}\right]\sqrt{\frac{\rho^r}{\rho^r+\ell_3}}\, e^{-jk\ell_3};$$

for $\tilde{P}$ in the lit region. (A-12a)

$$\tilde{u}_3(\tilde{P}) \sim \tilde{u}_3^i(Q_a)\left[-\sqrt{m(Q_a)m(Q_b)}\ e^{-jkt_3}\sqrt{\frac{2}{k}}\left\{\frac{e^{-j\frac{\pi}{4}}}{2\sqrt{\pi}\,\xi^d}\left[1-F(X^d)\right] + \hat{P}_{\substack{s\\h}}(\xi^d)\right\}\right]\frac{e^{-jks_3}}{\sqrt{s_3}} \ ;$$

for $\tilde{P}$ in the shadow region. (A-12b)

The ρ^r appearing in Equation (A-12a) is given by

$$\rho^r = \tilde{\rho}_t^r/\sin\theta_0 = \left(\frac{\rho_\tau}{\sin^2\theta_0}\right)\frac{\cos\theta^i}{2} \quad . \tag{A-13}$$

The result of Equations (A-10;b) or (A-12a;b) is valid outside the paraxial regions of the cylinder; i.e., it is valid for θ_0 not close to 0^0 or 180^0.

One may view the incident field $\tilde{u}_3^i$ as being produced by a scalar point source at the point P ($P=P_L$ or $P=P_S$) which receeds to infinity. If the strength of this source is a_0, then:

$$u_3^i(Q_R) \sim a_0\left(c\,\frac{e^{-jks_3^r}}{s_3^r}\right); \qquad \tilde{u}_3^i(\tilde{P})\Big|_{\text{lit zone}} \sim a_0\, c\,\frac{e^{-jks_3^r}}{s_3^r}\, e^{-jk(s_3^i-s_3^r)}$$

(A-14a;A-14b)

$$\tilde{u}_3^i(Q_a) \sim a_0\left(c\,\frac{e^{-jks_3^d}}{s_3^d}\right); \qquad \tilde{u}_3^i(\tilde{P})\Big|_{\substack{\text{shadow}\\ \text{zone}}} \sim a_0\, c\,\frac{e^{-jks_3^d}}{s_3^d}\, e^{-jk(s_3^i-s_3^d)} \quad .$$

(A-14c;A-14d)

The incident field u_3^i may be normalized to a unit spherical wave by suppressing the factor $c\,\frac{e^{-jks_3{}'^d}}{s_3{}'^d}$ for the case of "plane wave incidence".

Let a scalar point source of strength b_0 placed at P of Figure A-1 generate an incident field u_3^i with the source at P (i.e., $P=P_L$ or $P=P_S$) turned off. The total far zone field u_3 of this source in the presence of the cylinder is also obtainable from $\tilde{u}_3$ of Equations (A-12a;b) via reciprocity and is given by

$$b_o\,\tilde{u}_3(\tilde{P}) = a_o\,u_3(P) \quad ; \begin{cases} P=P_L \;, & \text{if } \tilde{P} \text{ is in the lit zone} \\ (P_L \to \infty) & \\ P=P_s \;, & \text{if } \tilde{P} \text{ is in the shadow zone.} \\ (P_{s\to\infty}^{s}) & \end{cases}$$

(A-15)

It follows after some re-arrangement of terms that:

$$u_3(P_L) \sim u_3^i(P_L) + u_3^i(Q_R)\left[-\sqrt{\frac{-4}{\xi^L}}\, e^{-j(\xi^L)^3/12}\left\{\frac{e^{-j\frac{\pi}{4}}}{2\sqrt{\pi}\,\xi^L}\left[1-F(X^L)\right]+\hat{P}_{\substack{s\\h}}(\xi^L)\right\}\right]\sqrt{\rho_1^r\,\rho_2^r}\,\frac{e^{-jks_3^r}}{s_3^r}\;;$$

for $P=P_L$ in the lit zone. (A-16a)

$$u_3(P_s) \sim u_3^i(Q_b)\left[-\sqrt{m(Q_b)m(Q_a)}\; e^{-jkt_3}\sqrt{\frac{2}{k}}\left\{\frac{e^{-j\frac{\pi}{4}}}{2\sqrt{\pi}\,\xi^d}\left[1-F(X^d)\right]+\hat{P}_{\substack{s\\h}}(\xi^d)\right\}\right]\sqrt{\frac{d\eta(Q_b)}{d\eta(Q_a)}}\cdot\sqrt{\rho_c}\,\frac{e^{-jks_3^d}}{s_3^d}\;;$$

for $P=P_s$ in the shadow zone. (A-16b)

In the above solution of Equations (A-16a;b) for the reciprocal or the point source excitation problem, all the ray directions in Figures (A-1a;b) must be reversed. Also, ξ^d and t_3 must be defined as

$$\xi^d = \int_{Q_b}^{Q_a} \frac{m(t')}{\rho_g(t')}\,dt' \quad ; \qquad t_3 = \int_{Q_b}^{Q_a} dt' \;. \qquad \text{(A-17a;A-17b)}$$

The quantities, ρ_1^r and ρ_2^r represent the reflected ray caustic distances for the point source excitation case.

$$\frac{1}{\rho_1^r} = \frac{1}{\ell_3} + \frac{1}{\rho^r} \quad ; \qquad \frac{1}{\rho_2^r} = \frac{1}{\rho_3} \;. \qquad \text{(A-18a;A-18b)}$$

The ρ^r in Equation (A-18a) is defined in Equation (A-13). The quantities $\rho_{1,2}^r$ can be obtained via Equation (6a) of Section II-A. The quantities within the radical signs outside the square brackets of Equation (A-16b) are defined as

$$\frac{d\eta(Q_b)}{d\eta(Q_a)} = \frac{s_3}{s_3+t_3} = \begin{pmatrix}\text{surface ray}\\ \text{divergence}\\ \text{factor}\end{pmatrix}^2 \quad ; \quad \rho_c = s_3+t_3 = \begin{matrix}\text{caustic distance}\\ \text{for the surface}\\ \text{diffracted ray}\end{matrix} \; .$$

(A-19a;A-19b)

It is understood that the following far zone approximations are implied in Equations (A-16a;b):

$$u_3^i(P_L) \sim b_o \, c \, \frac{e^{-jks_3^r}}{s_3^r} \, e^{-jk(s_3^i - s_3^r)} \quad ; \quad u_3^i(Q_R) \sim b_o \, c \, \frac{e^{-jk\ell_3}}{\ell_3} \; ; \quad u_3^i(Q_b) \sim b_o c \, \frac{e^{-jks_3}}{s_3}$$

(A-20a;A-20b;A-20c)

$$u_3^i(P_s) \sim b_o c \, \frac{e^{-jks_3^d}}{s_3^d} \, e^{-jk(s_3^i - s_3^d)} \; . \qquad \text{(A-20d)}$$

In conclusion, Equations (A-16a;b) represent the far zone field of a scalar point source at $\tilde{P}$ (see Figure 1a;b) which radiates in the presence of a convex cylinder. If one suppresses the spherical wave factor $c\, e^{-jks_3^{r,d}}/s_3^{r,d}$ in Equations (A-16a;b), one then obtains the "total far field pattern" of that point source in the presence of the cylinder.

ACKNOWLEDGMENT

The work reported in this report was partially supported by Joint Services Electronic Program Contract N00014-78-C-0049 between Department of the Navy, Office of Naval Research, and The Ohio State University Research Foundation.